A unified design method for 2D auxetic metamaterials based on a minimal auxetic structure

Roberjot, Pierre; Herder, Just L.

DOI
10.1016/j.ijsolstr.2024.112777

Publication date
2024

Document Version
Final published version

Published in
International Journal of Solids and Structures

International Journal of Solids and Structures 295 (2024) 112777

Contents lists available at ScienceDirect

International Journal of Solids and Structures

journal homepage: www.elsevier.com/locate/ijsolstr

A unified design method for 2D auxetic metamaterials based on a minimal auxetic structure

Pierre Roberjot *, Just L. Herder

Delft University of Technology, Department of Precision and Microsystems Engineering, Mekelweg 2, 2628CD, Delft, The Netherlands

ARTICLE INFO

Keywords:
Auxetic
Metamaterials
Poisson's ratio
Rational design

ABSTRACT

Auxetic metamaterials are architected structures that possess a unique property known as a negative Poisson's ratio. This remarkable characteristic enables them to expand or contract in a direction perpendicular to stretch or compression. Due to their exceptional attributes such as energy absorption and fracture resistance, these auxetic metamaterials hold great promise for various applications across multiple domains.

However, the widespread development of these materials has been hindered by the absence of an efficient design method. Addressing this limitation, our work introduces a minimal 2D auxetic structure and a corresponding design approach that comprises two geometric transformations. This design method not only allows for the replication of existing auxetic structures but also facilitates the creation of novel structures. Additionally, it enables the classification of these structures into six distinct categories.

To enhance the understanding and standardization of these structures, we propose a naming protocol and define their associated unit cell. Furthermore, we explore the possibilities of tessellations within this framework. Finally, we examine the auxetic structures from the perspective of surface strain, which is closely linked to the Poisson's ratio, the Bulk modulus and compressibility.

1. Introduction

Over the past few decades, mechanical metamaterials have emerged as a new class of materials due to their architected structures which enable them to possess exotic behaviors (Frenzel et al., 2017; Kadic et al., 2019; Fernandez-Corbaton et al., 2019). Unlike conventional materials, auxetic structures have a negative Poisson's ratio (NPR), which means they expand in transverse directions when stretched along the longitudinal axis. This unusual behavior has led to a wide range of potential applications, including impact-resistant materials (Giacomin et al., 2006; Zhang et al., 2020; Ji et al., 2021), strong low-density structures (Wang et al., 2016; Yousefi et al., 2022), advanced filters (Alderson et al., 2002), sensors (Lee et al., 2010; Jiang et al., 2018; Ye et al., 2022; Taherkhani et al., 2023; Cuthbert et al., 2023), tissue engineering (Flamourakis et al., 2020; Yarali et al., 2023), medical (Ali and Rehman, 2011; Ali et al., 2014; Lee et al., 2016; Wu et al., 2018), wearable devices (Rant et al., 2013; Papadopoulou et al., 2017; Duncan et al., 2018; Faraci et al., 2021; Namvar et al., 2023), and stretchable electronics (Jang et al., 2022).

In 1985, the first auxetic structures were created in foams with a 3D re-entrant structure (Kolpakov, 1985; Lakes, 1987; Zhang et al., 2023; Ren et al., 2023). Since then, auxetic structures have gained considerable research attention. Isotropic materials have a Poisson's ratio (PR) in the range between −1 and 0.5. While some materials have positive PR, such as rubber (ν = 0.499), copper (ν = 0.330), and steel (ν = 0.285), cork has a PR of zero, meaning it maintains its thickness when stretched. The rare instances of natural auxeticity were found recently in structures such as tendons (Gatt et al., 2015b), and bones (Williams and Lewis, 1982). In contrast, the auxetic behavior in artificial materials is typically engineered into the structure, with the most common architecture being the re-entrant honeycomb or bow-tie structure (Wang et al., 2017; Li et al., 2019; Lim, 2019; Wu et al., 2021; Khoshgoftar et al., 2022). Over time, more complex and modified structures have been developed, such as the double arrowhead (Larsen et al., 1997; Kolken and Zadpoor, 2017), connected stars (Grima et al., 2005b), and rotating triangles (Grima et al., 2005a, 2011; Papadopoulou et al., 2017). Auxetic structures can possess a chiral geometry (Jiang and Li, 2017, 2018), leading to chiral and anti-chiral structures such as the missing-rib (Smith et al., 2000; Zhu et al., 2022a), chiral honeycombs (Zhang et al., 2022b), and some auxetic fibers (Sloan et al., 2011; Ge et al., 2016; Ng and Hu, 2017; Cuthbert et al., 2023). Most auxetic structures have a NPR between 0 and −1, but some have shown a PR below −1, with values as low as −16 (Shaat and Wagih, 2020), −17 (Dirrenberger et al., 2011), and even reported to be −100 (Domaschke et al., 2019) for very small strains. While the

* Corresponding author.
E-mail addresses: P.Roberjot@tudelft.nl (P. Roberjot), J.L.Herder@tudelft.nl (J.L. Herder).

https://doi.org/10.1016/j.ijsolstr.2024.112777
Received 2 September 2023; Received in revised form 26 February 2024; Accepted 15 March 2024
Available online 22 March 2024

isotropic definition is sufficient to describe natural auxetic structures, it is not suitable for describing most of artificial auxetic materials or metamaterials. Achieving a lower PR is typically accomplished through large deformation or by adding anisotropy to the structure's design.

Despite their promising potential, the lack of efficient design methods for auxetic metamaterials has hindered their widespread application. Currently, trial-and-error methods are often used to develop these materials, resulting in inefficient and time-consuming processes. Therefore, the development of efficient design methods (Grima et al., 2005b; Stavric and Wiltsche, 2019; Broeren et al., 2019; Liu et al., 2022) for auxetic metamaterials is essential for advancing their practical applications. In addition, the trial-and-error design of auxetic metamaterial prevents the elaboration of a general organic classification (Alderson and Alderson, 2007; Liu and Hu, 2010; Lim, 2020; Hu and Zulifqar, 2017).

In this paper, we present a structural and topological design method for both existing and novel 2D auxetic metamaterials based on a simple minimal auxetic structure. Our design method in three steps, uses two geometrical transformations and, creates three achiral and three chiral 2D auxetic groups. We first propose the topology of a minimal auxetic chiral metastructure, we calculate the strain and Poisson's ratio behavior. We then propose a three-step design method that enable to classify auxetic structures with their chirality, we introduce a naming protocol that encodes the transformations applied to the minimal auxetic structure. Next, we use the design method to create six auxetic groups, including higher order regular and irregular geometrical structures. We introduce a protocol for the creation of the unit cells and a way to tessellate planar auxetic metastructures in a regular and non regular tiling. Lastly, we suggest observing the auxetic structures with surface strain, a more general metric that directly links to the bulk modulus and compressibility of the metamaterial.

2. Methods

In this section we are first proposing a classification of the auxetic structures from the chirality point of view, second we present a base chiral auxetic structure and detailing the calculation of its strain, third we construct three base achiral structures from the chiral base and finally we propose a design protocol for the creation of planar auxetic metamaterials along with a naming and nomenclature protocol.

2.1. Poisson's ratio metamaterials and a minimal auxetic metastructure

The Poisson's ratio (ν) is defined as the negative ratio of transverse ($\varepsilon_{\text{trans}}$) and longitudinal ($\varepsilon_{\text{long}}$) strains:

$$\nu = -\frac{\varepsilon_{\text{trans}}}{\varepsilon_{\text{long}}} \tag{1}$$

For isotropic materials, ν falls within the range of -1 to 0.5. The strain in one direction is determined by the initial (L_I) and final (L_F) lengths:

$$\varepsilon = \frac{L_F - L_I}{L_I} = \frac{L_F}{L_I} - 1 \tag{2}$$

Poisson's ratio metastructures can be distinguished by the sign of their Poisson's ratio. Auxetic structures exhibit a negative Poisson's ratio (NPR), expanding in the direction normal to traction or contracting in the direction normal to compression. Anepirretic structures possess a Poisson's ratio of zero (ZPR), maintaining constant width under traction or compression. Meiotic structures, with a positive Poisson's ratio (PPR), narrow under traction and widen under compression (Dagdelen et al., 2017).

Metastructures, defined as architected structures or material mechanisms exhibiting exotic properties, can be tessellated or tiled. Tessellation is achieved by defining the contour of the architected structure, the unit cell (see Section 3.4). Metamaterials, being tessellations of metastructures, consist of repeated unit cells.

Metastructures and metamaterials, that are intended to be used as materials, conflict with isotropic materials when assigning material properties. Hence, we propose assigning metamaterial properties, or meta-properties, to the unit cell containing the material mechanism. For instance, the "meta" Poisson's ratio ν_m (with the index m indicating the metamaterial property) represents the deformation ratio of the entire metastructure unit cell. The Poisson's ratio of a metamaterial can be expressed as:

$$\nu_m = -\frac{\varepsilon_{trans_m}}{\varepsilon_{long_m}} \tag{3}$$

2.1.1. A chiral classification of auxetics

Chirality plays a crucial role in the characteristics of metamaterials, particularly in the context of Poisson's ratio metamaterials. A structure is deemed *chiral* when its configuration cannot be perfectly superimposed with its mirror image through any rotation in the plane. The chiral structure and its mirror image, known as the anti-chiral form, are referred to as the two *enantiomorphs* of the structure. Chirality is indicative of a twist orientation within a structure, allowing it to be categorized as either right or left-oriented. Conversely, a structure lacking chirality is termed *achiral*.

Certain auxetic structures exhibit chirality, implying that all others must inherently be achiral. Grouping auxetic structures based on their chirality provides an initial classification, distinguishing those with and without an internal twist. In addition, chirality is a complete and mutually exclusive classification.

Upon combining two enantiomorphs, the resulting structure becomes achiral, possessing a single axis of symmetry. In essence, an achiral structure with N axes of symmetry can be dissected into N chiral sub-structures.

Our hypothesis posits the existence of a minimal chiral auxetic structure. This structure would not only be auxetic but also form the building blocks for both chiral and achiral auxetic structures. The identification of such a minimal auxetic metastructure could significantly enhance our comprehension of existing planar auxetic structures and pave the way for the development of novel auxetic metastructures.

2.1.2. A minimal chiral auxetic metastructure

The bow-tie structure (Li et al., 2019), a prevalent auxetic configuration, is achiral and exhibits two axes of symmetry. Our proposal involves dividing this bow-tie structure into four parts, resulting in a "Z"-shaped structure as depicted in Fig. 1.a. This Z structure consists of a three-bar kinematic chain interconnected by revolute joints, as illustrated in Fig. 1.b, detailing the topological parameters of the kinematic structure. The Z structure features three rigid beams ($A'A = a_1$, $AB = a_2$, and $BB' = a_3$) and two angles ($\widehat{A'AB} = \theta_1$ and $\widehat{ABB'} = \theta_2$). For simplicity, we assume $a_1 = a_3$ and $\theta_1 = \theta_2$. The center of symmetry of the Z structure is denoted as O.

The Z structure is capable of extension or compression along the line A′B′, represented by sliders positioned at points A′ and B′. This kinematic arrangement yields one degree of freedom (DoF), determined by Grubler's mobility equation. We will consider in this manuscript that the structures presented possess a perfect auxetic behavior, for instance, they expand or compress in all direction evenly.

The Z structure is inherently one-dimensional since the positions of points A and B change during compression or extension, preventing perfect tessellation in the transverse direction. However, points A′ and B′ slide along the line A′B′ passing through point O, allowing connection along this line. To tessellate two Z structures, one can connect Z_1 and Z_2 at points B'_1 and A'_2, respectively. The unit cell of Z is constructed from the lines normal to (A′B′) at the points A′ and B′, and the lines parallel to (A′B′) crossing the points A and B. The unit cells are illustrated in Fig. 1.c for an arbitrary angle θ and in Fig. 1.d at the maximum value of the angle $\theta = \theta_{max}$, where the auxeticity is maximum.

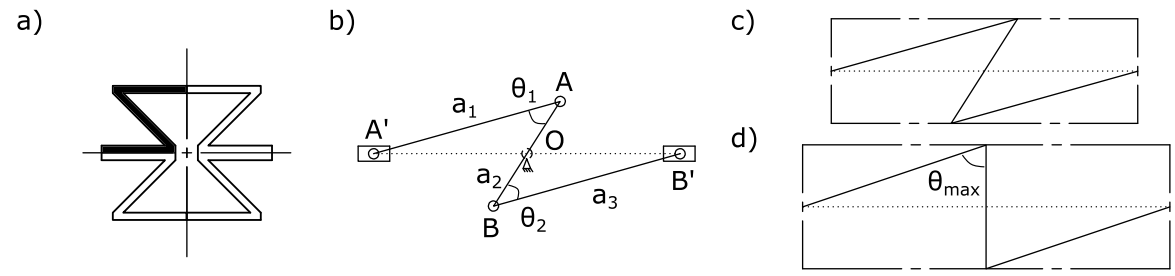

Fig. 1. (a) The bow-tie structure with the two axes of symmetry and in black, the Z structure, (b) representation of the mechanism and the parameters of the Z structure, (c) the representation of the unit cell of Z and (d) the unit cell when the angle θ is at the value of the maximum of the auxeticity.

2.1.3. Strains and Poisson's ratio of Z

The Z structure is auxetic in the range of the angle $\theta \in [0°, \theta_{max}]$, indeed, the structure can be compressed to a theoretical minimum, where $\theta = 0°$. In this configuration the length of Z is $L = a_1 + a_3 - a_2$, and with $a_1 = a_3$, the length becomes

$$L(0) = 2a_1 - a_2 \tag{4}$$

and the height H is minimum, if the beams are considered having a negligible thickness h, $H = 3h \approx 0$.

When $\theta = \theta_{max}$ the triangle A′AO has a right angle at O, therefore θ_{max} can be derived with trigonometry:

$$cos(\theta_{max}) = \frac{[AO]}{[A'A]} \tag{5}$$

with $[AO] = a_2/2$ and $[A'A] = a_1$, thus,

$$cos(\theta_{max}) = \frac{a_2}{2a_1} \tag{6}$$

The value of θ_{max} gives a limitation on the dimensions of Z, $a_2 \leq 2a_1$. At this state, the height is maximum $H_{max} = H(\theta_{max}) = a_2$. The length $[A'B']$ can be decomposed as $[A'B'] = [A'O] + [OB'] = 2[A'O]$, and can be calculated with Pythagoras's formula

$$a_1^2 = \left(\frac{a_2}{2}\right)^2 + [A'O]^2 \tag{7}$$

which yields to,

$$[A'O] = \sqrt{a_1^2 - \frac{a_2^2}{4}} \tag{8}$$

The length at θ_{max} is

$$L(\theta_{max}) = 2\sqrt{a_1^2 - \frac{a_2^2}{4}} \tag{9}$$

To calculate the length of Z for every θ, one could calculate the length $L(\theta) = 2[A'O]$. [A'O] belongs to the random triangle A′AO, hence the Al-Kashi law can be used,

$$[A'O]^2 = a_1^2 + \left(\frac{a_2}{2}\right)^2 - 2a_1\frac{a_2}{2}cos(\theta) \tag{10}$$

The length of the unit cell of Z can be derived for all θ as

$$L(\theta) = 2\sqrt{a_1^2 + \left(\frac{a_2}{2}\right)^2 - a_1 a_2 cos(\theta)} \tag{11}$$

The values of $L(O)$ and $L(\theta_{max})$ can be found with this equation.

The calculation of the height is done with the law of sines, the values of a_1, a_2 are fixed and θ is known, thus the angle $\widehat{AA'O}$ can be determined

$$\frac{2sin(\widehat{AA'O})}{a_2} = \frac{2sin(\theta)}{L(\theta)} \tag{12}$$

which can be written

$$sin(\widehat{AA'O}) = \frac{a_2 sin(\theta)}{L(\theta)} \tag{13}$$

and using trigonometry in the right triangle A′AO′, with O′ the projection of A in the line (A′B′), the height can be derived as

$$H(\theta) = a_1 sin(\widehat{AA'O}) = \frac{a_1 a_2 sin(\theta)}{L(\theta)} \tag{14}$$

Knowing the length $L(\theta)$ (Eq. (11)) and the height $H(\theta)$ (Eq. (14)), one can calculate the longitudinal ($\varepsilon_L(\theta)$) and transversal ($\varepsilon_H(\theta)$) strain.

$$\begin{aligned} \varepsilon_L(\theta) &= \frac{L(\theta)}{L_I} - 1 \\ \varepsilon_H(\theta) &= \frac{H(\theta)}{H_I} - 1 \end{aligned} \tag{15}$$

with L_I and H_I representing the values of length and height at θ_I, the initial state of Z. The longitudinal and transverse strain are plotted in Fig. 2.a,b as a function of θ for three couples of value of $[a_1, a_2]$. The Poisson's ratio ($\nu(\theta)$) as a function of θ can be written

$$\nu(\theta) = -\frac{\varepsilon_H(\theta)}{\varepsilon_L(\theta)} \tag{16}$$

The evolution of the Poisson's ratio is shown as a function of θ in Fig. 2.c for different values of a_1 and a_2, with an initial angle $\theta_I = 20°$ taken arbitrarily.

2.2. Design protocol of auxetic structures

We have been proposing the Z structure, a three-bar linkage structure, as a possible minimal chiral auxetic structure. We have shown how to find the Z in the bow-tie auxetic metastructure and we demonstrated that Z is also presenting an auxetic behavior. We are proposing a design protocol that uses the Z metastructure as an input and generates topological design of auxetic structures. The design method, illustrated in Fig. 3.a, is a three-step protocol composed of two topological transformations.

The first transformation is called the "achiralisation" process. It consists in joining the two enantiomorphs of a chiral object together to create an achiral structure. The transformation is illustrated in Fig. 3.b.

The second transformation is the "copy-rotation" process. It consists in copying an object N times and locating them equally around a point of rotation O_R and linked together. Each object is lying in one of the N sectors thus created, each of the sector possessing an angle

$$\varphi_N = \frac{360°}{N} \tag{17}$$

The transformation is illustrated in Fig. 3.c.

In addition to these two topological transformations a set of four rules needs to be respected in order for the design process to work efficiently.

Rule 1. The Z structure is composed of rigid beams linked by revolute joints,

Rule 2. The edges A′ and B′ of Z are joined rigidly by the achiralisation, copy-rotation and tessellation transformations,

Rule 3. The dimensions of the beams (a_1, a_2, and a_3) and the angles of Z (θ_1 and θ_2), can be changed,

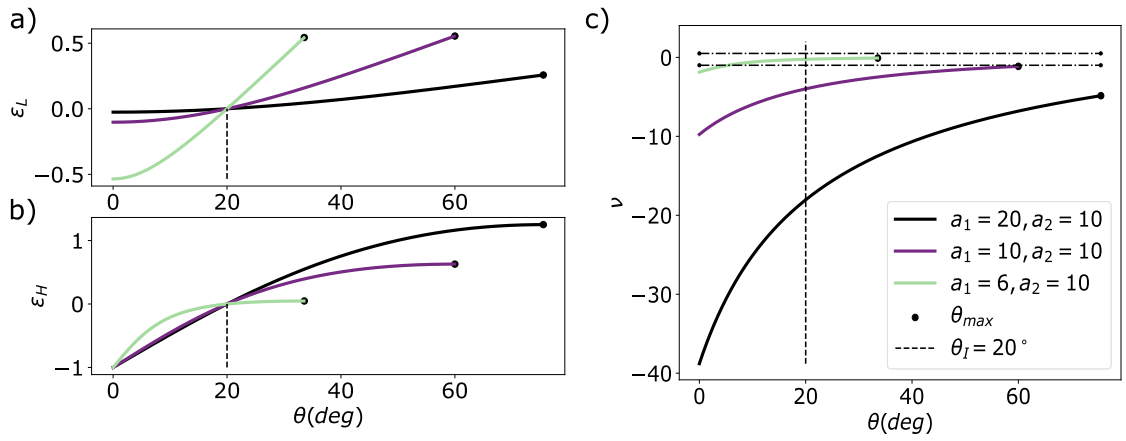

Fig. 2. Evolution of the (a) longitudinal strain (ε_L), (b) the transverse strain (ε_H), and (c) the Poisson's ratio (ν) for three couples $[a_1, a_2]$ of dimensions of Z, with an initial angle $\theta_I = 20°$. The horizontal dotted lines (.-.) represent the isotropic limit of the Poisson's ratio $]-1, 0.5[$.

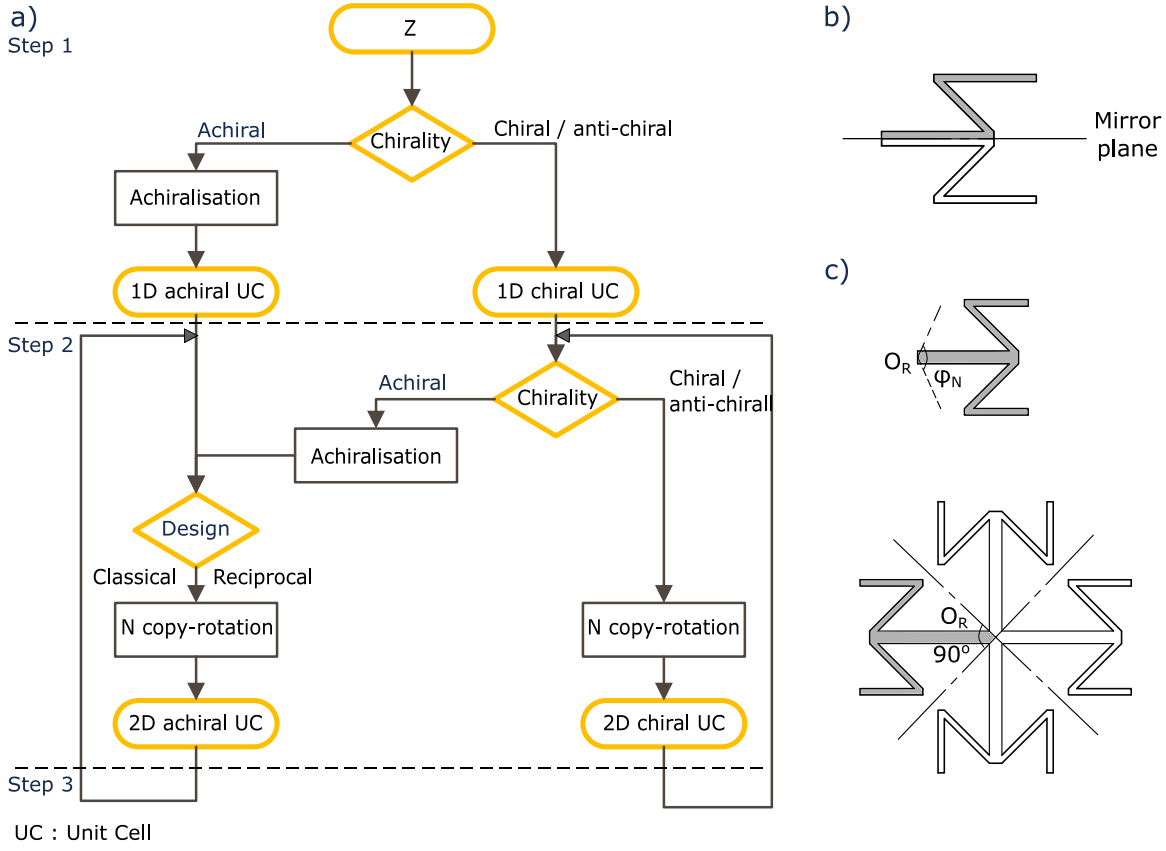

Fig. 3. Representation of (a) the flow diagram of the design method for 2D auxetic structures with the illustration of (b) an example of the achiralisation process, for the Z structure and (c) an example of the copy-rotation process for the "connected star" reciprocal design with 4 base achiral elements.

Rule 4. The revolute joints can be superimposed during the achiralisation and copy-rotation transformations.

The design method combines the two topological transformations in three steps to generate auxetic metastructures.

The first step consists in defining the chirality of the base structure. If the base structure is chiral, no transformation is applied to the Z. If the base structure is achiral, thus the achiralisation process is applied to the Z, we present three remarkable achiral bases in Section 3.1.1. The output of the first step is the creation of 1D (or 1.5D) auxetic structures, because all the edges E are colinear, and can be tessellated only as a line.

The second step have two possible inputs, first an achiral structure, the achiral base can be copy-rotated, however two options are permissible. The design can be "classical" or "reciprocal" before applying the copy-rotation protocol. A classical structure possess one edge point E_N per sector S_N, whereas the reciprocal structures possess two edges points E_{N1} and E_{N2} per sector S_N. For the higher-order metastructures, a classical design is defined as the side of the achiralised structure that possess the equivalent edge E closer to the edge points E_n of the metastructure, oppositely, the reciprocal design is possess the equivalent edge E the furthest to the edge points E_n. The higher-order classical and reciprocal are illustrated in Section 3.3. Second, the structure is chiral, the input is therefore the Z. A chiral structure cannot be classical

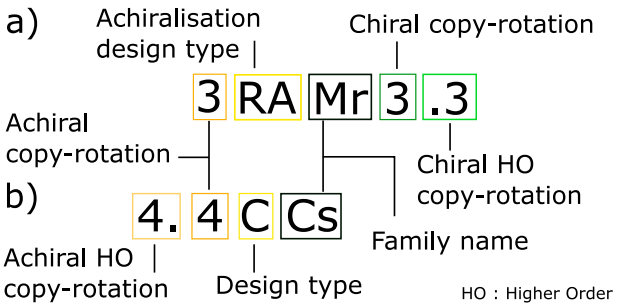

Fig. 4. The details of the code for (a) chiral and, (b) achiral auxetic metastructures.

nor reciprocal, it will consist of using one of the two enantiomorphs. The copy-rotation process is applied to the Z directly. The second step allows the creation of six remarkable families, three of which are achiral (Section 3.1), the other three are chiral (Section 3.2). The type of design and center of rotation O_R are defined for each families. The output of the second step is a 2D metastructure that can be tessellated in the plane.

The third step is looping over the second step with, as input a 2D metastructure, generated by the second step. The loop can be repeated an infinite number of times and brings the creation of higher order auxetic structures (Cf. Section 3.3). A chiral structure can be achiralised in the third step to create a higher-order achiralised metastructure, or copy rotated to create a higher-order copy-rotated metastructure, which applies to the achiral structures too.

2.3. Naming and nomenclature protocol for auxetic structures

We have proposed a design protocol consisting of two design processes that allow the creation of both existing and novel auxetic structures. These processes can be used to pursue the design of auxetic base structures to an infinite number of structures. To enable referencing these structures, a naming protocol is proposed. Our naming protocol is encoding the topological transformations applied to Z to generate any design following the design method. The name given to auxetic structures are coded as presented in Fig. 4, and illustrated in Appendix F.

First, the design method produces six families of auxetic structures, which include the existing and novel structures, and as illustrated in Section 3, three of which are achiral, the "Connected stars" (Cs), the "Puzzle tiles" (Pt), and the "Rotating triangles (Rt). The three others are chiral families, the "Honeycomb" (Hc), the "Missing rib" (Mr), and the "Closed geometry" (Cg). The family names are abbreviated by two letters which are defining the chirality, the position of the remarkable axes of achiralisation, and the position of the remarkable center of rotation O_R.

Second, the naming protocol is the following, it defines steps to name a planar auxetic structure,

Step 1. The family name is the base of the coded name, it encodes the chirality, the axes of achiralisation and the position of the center of rotation O_R,
Step 2. All chiral copy-rotations are written on the right of a chiral name, higher-order copy-rotations are separated with a dot ".",
Step 3. A chiral structure which is achiralised is noted with a "A" on the left of the name,
Step 4. Achiral base structures possess a classical "C" or reciprocal "R" design, the type of design is written on the left of the achiral name,
Step 5. All achiral copy-rotations are written on the left of the achiral name, higher-order copy-rotations are separated with a dot ".".

An auxetic metastructure is constructed from a given name by first reading the family name, then the chiral transformations, and finally the achiral transformations.

A chiral structure, for instance, the missing rib design Mr, is copy-rotated three times, giving the Mr3 structure. If Mr3 is copy-rotated to the higher-order three times again, this yields to the structure Mr3.3. Mr3.3 can be achiralised to AMr3.3 and copy-rotated, as a reciprocal design, for instance 3 times to give 3RAMr3.3 the result is shown in Fig. 13.e.

An achiral structure such as the connected stars Cs can only be copy-rotated in the achiral form. For instance, four copy-rotation of Cs in the classical form leads to 4CCs and a four times higher-order copy-rotation leads to 4.4CCs as illustrated in Fig. 12.j.

3. Applications of the design method, tessellation, naming and metric of auxetic structures

We have proposed a minimal chiral auxetic metastructure, we have shown that this three-bar linkage present interesting large Poisson's ratio properties. We proposed a design method that enables the design of existing and novel auxetic structures, along with a naming protocol that encodes the transformations applied to the base structure Z.

In this section, we illustrate the design method. We show first the achiralisation of the Z structure to shape the three base achiral structures, and second apply the copy-rotation protocol to these achiral, and to the Z structure. Third, we illustrate the higher-order transformations. Then, we propose a method to design the unit cells of the designed auxetic structures. We finally present the surface strain as a metric for auxetic metamaterials.

3.1. Building achiral structures

Here we first introduce how to use the achiralisation process to the Z to create the base achiral auxetic structures. Second we illustrate how to use the copy-rotation on the achiral base structures, how to define the center of rotation O_R the edges E and how to design classical and reciprocal structures.

3.1.1. Construction of base achiral auxetic structures

The first step of the design protocol allows to achiralize the Z structure to create achiral base auxetic structures.

Z is a chiral structure, thus possesses two enantiomorphs, Z and its mirrored image (Fig. 5.a). The two enantiomorphs can be joined to form achiral structures. In other words, axes of symmetry can be chosen around the Z structure, and, combining the two mirrored structures a new achiral auxetic structure can be created. We present in Fig. 5 three remarkable axes of symmetry and build three base auxetic structures. These axes are remarkable because they enable to design existing structures, however, any variation from these axes is possible and brings small variation of the design.

As stated above, the Z is composed of rigid beams linked by revolute joints, and when two beams are linked by an axis of symmetry they form one single rigid element. The rules of topological construction of the auxetic structures are detailed in Section 2.2.

The first achiralisation, designed as "Connected stars", Fig. 5.b, is mirroring Z from the line (A′A) or (B′B). It generates one half of the re-entrant auxetic structure (Almgren, 1985). The structure is fully deployed when it reaches its maximum auxeticity, meaning that the angles θ are maximum $\theta_{max} = 90°$. The family of the Cs structure is presented in Section 3.1.2.

The second achiralisation, designed as "Puzzle tiles", depicted in Fig. 5.c, is mirroring Z from a line normal to (A′A) passing thought the point A′ (or normal to (B′B) and passing through B′). The structure is fully deployed when the angles θ are maximum $\theta_{max} = 90°$. The family of the Pt structure is presented in Section 3.1.3.

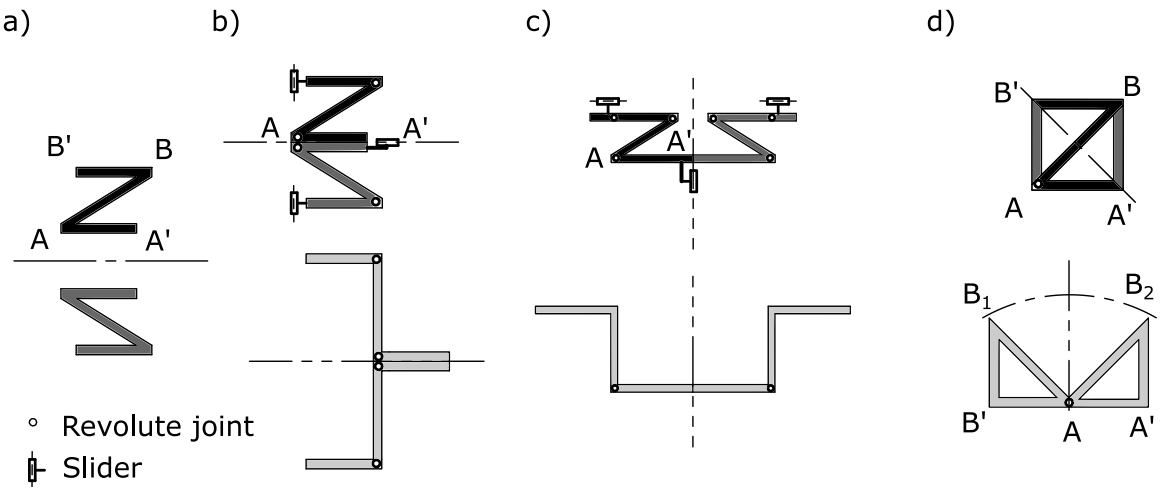

Fig. 5. Topology and parameters of (a) the two enantiomorphs, in black and dark gray, of the chiral Z metastructure. The representation of the achiral bases, from the first step of the design method, with on the top the undeformed and at the bottom the deformed (in light gray) topology, of (b) the connected stars base, (c) the Puzzle tiles base, and (d) the rotating triangles base.

The third achiralisation, called "Rotating triangles", is mirroring Z from the line (A′B′), this results in creating a square structure that is composed of two right triangles ABA′ and ABB′. As stated above, two beams that are linked by an axis of symmetry create a rigid body, thus, the beams A′A and A′B are forming one rigid triangle AA′B, as for the lines B′B and AB′ that create a rigid triangle AB′B. The two triangles are joined at the point A, and the revolute join B is removed, and split in two points B_1 and B_2, to allow the triangles to rotate. The topology and kinematics are represented in Fig. 5.d, the family of Rt is presented in Section 3.1.4. The maximum of auxeticity of the base structure is achieved when the angle between the two triangle $\alpha = 90°$, in the general case it depends on the order of the copy-rotation (see Section 3.1.4). The regular design is forming a square structure form two rights triangles, this design correspond also to the base structure of the 2 and 4 copy-rotations of the family. The Rt family is also display two non-right triangles for other N copy-rotation, the example of the 3CRt and 3RRt structure is illustrated in Fig. 8.c and f.

3.1.2. Achiral auxetic connected stars

Auxetic "connected stars" (Grima et al., 2005b) (Cs) are one of the most common achiral auxetic metamaterials (Fu et al., 2016; Jiang et al., 2019; Lurie et al., 2018; Yao et al., 2023). The classical (CCs) structures can be created with the copy-rotation protocol from the achiral base Fig. 5.b, that is created by the x-axis symmetry of the Z element. The center of rotation O_R is created from the triangle $(A_1 O_R A_2)$, with the angle φ_N between the lines $(A_1 O_R)$ and $(A_2 O_R)$, and the edge E of the structure is located at the point $B'_1 = B'_2$ (Fig. 6.a). The case $N = 2$ is a symmetry of the base achiral structure from the axis $(A'_1 A'_2)$. Building the N-order connected stars (Fig. 6.b, c, and d), one uses the copy-rotation on the base structure around the center O_R and connects the points A_{1n} to $A_{2(n+1)}$, with $n \in [1, N]$. The beams $(A_1 A'_1)$ and $(A_2 A'_2)$ have, for $N \geq 3$, a length of $a_{1n} = a'_{1n} = 0$, with a_{1n} and a'_{1n} the length $[A_{1n} A'_{1n}]$ and $[A_{2n} A'_{2n}]$ of the copy-rotated structures. If the copy-rotation was based on the triangle $A'_1 O_R A'_2$, extra beams and revolute joints would have been in the structure, thus more internal degrees of freedom would have been present throughout the deformation, and the auxeticity might be lost in a non-ideal embodiment of the design.

A reciprocal design (Section 2.2) of the achiral connected stars (RCs) (Fig. 6.f, g, and h) are created from a second center of rotation created from the triangle $(A_1 O_R A_2)$ (Fig. 6.e), here the center of rotation O_R is the point B'. Two edges of the structure can be found $E_1 = A'_1$ and $E_2 = A'_2$, a constructed edge point E can be defined as the normal intersection of the line $(A'_1 A'_2)$ and $(B'E)$. The classical and reciprocal connected stars structures are fully deployed when the angles θ of all the N structures are deployed to their maximum, i.e. when $\theta = 90°$.

The reciprocal design with a 4 copy-rotation, referred to as 4RCs (Section 2.3), possesses an initial length L_I and height H_I, illustrated in Fig. 6.i. When stretched in the x direction, the length changes from L_I to a final length L_F, while the height remains constant (Fig. 6.j) due to the presence of a cross-like central rigid body.

This configuration results in an anepirretic behavior, characterized by $\nu = 0$ causing the strain $\varepsilon_x = (L_F - L_I)/L_I$ to be decoupled from the strain $\varepsilon_y = 0$. Similarly, the anepirretic and decoupled behavior is observed between the strain $\varepsilon_y = (H_F - H_I)/H_I$ and $\varepsilon_x = 0$ (Fig. 6.k). This anepirretic and decoupled behavior is also present in reciprocal connected star designs that have an even number of copy-rotation, starting from $N = 4$. These decoupled designs can be stretched from their opposite sectors without altering the shape of the unstretched configuration.

3.1.3. Achiral auxetic puzzle tiles

Auxetic "puzzle tiles" (Pt) are built from the base achiral structure depicted in Fig. 5.c. The center of rotation O_R, for the classical puzzle tiles (CPt), is created from the triangle $(A_1 O_R A_2)$, with the angle φ_N between the lines $(A_1 O_R)$ and $(A_2 O_R)$. The edge E of the structure is the center point of the beam $B_1 B_2$ (Fig. 7.a). The structure 2CPt gives a similar topology as 2CCs, they correspond both to one half of the bow-tie structure. For similar reasons as the Connected stars, the copy-rotation of CPt for $N \geq 3$ requires to have the length of the beams $A'_{1n} A_{1n} = a_{1n}$ and $A'_{2n} A_{2n} = a'_{1n}$ to be $a_{1n} = a'_{1n} = 0$. The topology of the classical structures of the Puzzle tiles are depicted in Fig. 7.b, c, d, the copy-rotated structures around the point of rotation O_R are connected rigidly at the points A_{1n} and $A_{2(n+1)}$, with $n \in [1, N]$.

As for the connected stars design, there exists a reciprocal design for the auxetic puzzle tiles (RPt). The center of rotation is also defined by the triangle $A'_1 O_R A'_2$ (Fig. 7.e), however, the points B_1, B_2, and B' are "inside" the triangle, and thus the lengths $A_1 A'_1$ and $A_2 A'_2$ need to be adapted not to have overlapping of the "inside" structures when the copy-rotation is applied. Two edges of the reciprocal structure can be found $E_1 = A_1$ and $E_2 = A_2$, the constructed edge E is defined as the normal intersection of the lines $(A'_1 A'_2)$ and $(O_R E)$. The reciprocal N-order puzzle tiles (Fig. 7.f, g, h), are built in the same manner as the classical ones connecting the points A'_{1n} to $A_{2(n+1)}$.

The classical and reciprocal connected puzzle tiles can be seen as a complementary design of the connected stars. Indeed, when tiled the connected stars and puzzle tiles are forming similar patterns, therefore, CPt and CCs have an auxetic behavior whereas RCs and RPt possess,

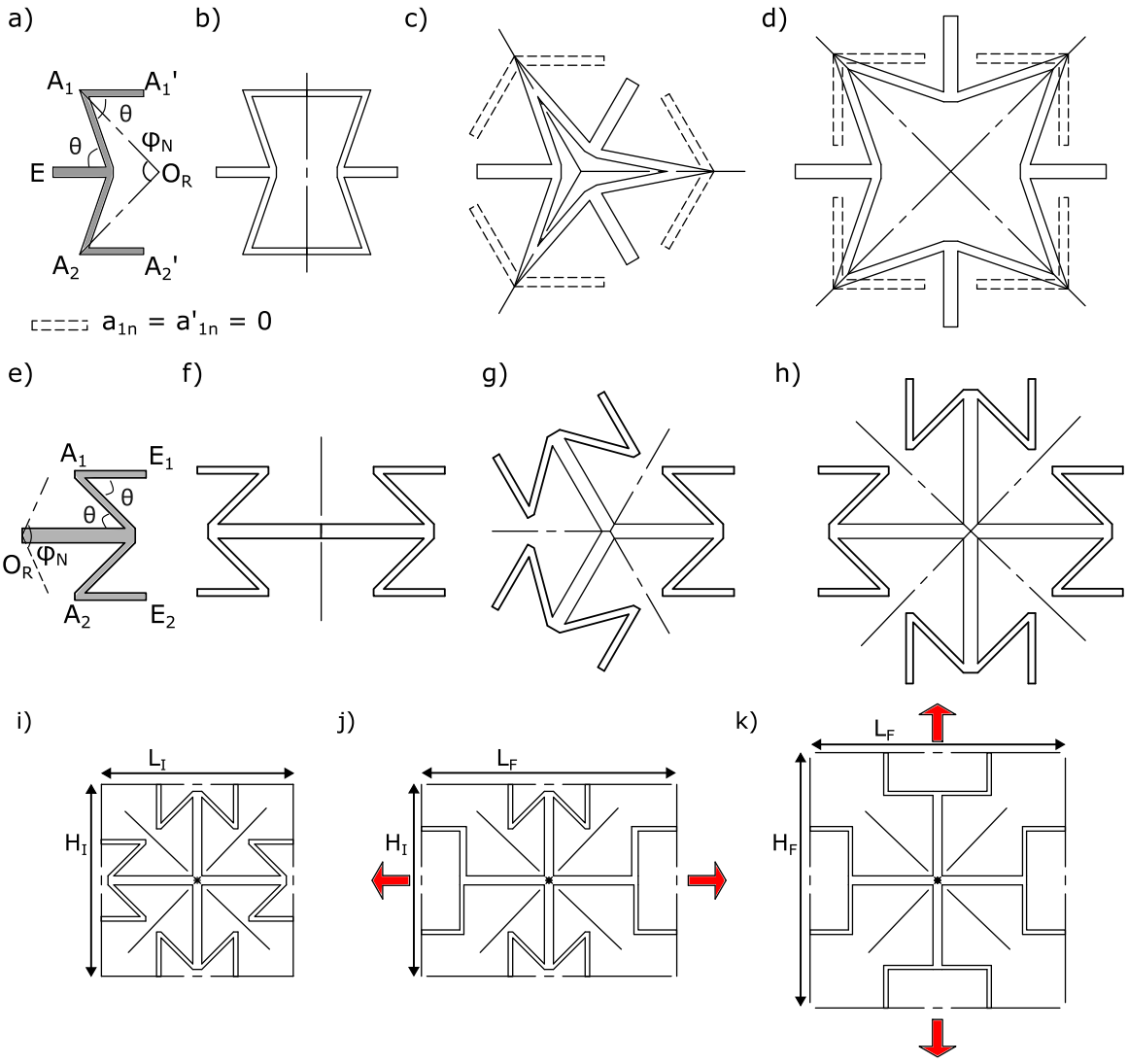

Fig. 6. Geometrical design of the regular achiral "connected stars" (Grima et al., 2005b), or re-entrant auxetic metamaterials, with (a) the construction of the center of rotation O_R and the representation of the cases (b) 2CCs where $N = 2$ (c) 3CCs where $N = 3$, and (d) 4CCs $N = 4$. The design of the reciprocal achiral connected stars, with (e) the construction of the center of rotation $O_R = B'$ and the edges E_1, E_2 and E, and representation of the geometries for (f) 2RCs where $N = 2$, (g) 3RCs where $N = 3$, and (h) 4RCs where $N = 4$. The design 4RCs (i) with the initial length L_I and height H_I, (j) 4RCs is stretched in the x direction, the final maximum length is L_F, however the height does not change which gives the anepirretic behavior, the strain in the x direction ϵ_x is uncoupled from the strain ϵ_y. (k) 4RCs is stretched in the y direction after being stretched in the x direction, the strain ϵ_y is also uncoupled from ϵ_x.

both, an anepirretic behavior. We present the puzzle tiles as a separate family because they could enable the creation of specific designs in the higher order or with irregularities added to the structures.

For instance, an irregular variation of the $N = 2$ puzzle tile is usually called the "arrowhead" auxetic design (Larsen et al., 1997; Boopathi et al., 2020), a detail of the symmetry and topology is depicted in Appendix A, the name "arrowhead", can be short for "Pt arrowhead".

3.1.4. Achiral auxetic rotating-triangles

The achiral auxetic "rotating-triangles" (Rt) is created from the base achiral structure as shown in Fig. 5.d. The center of rotation O_R is created from the triangle $(A'O_RB')$, with the angle φ_N between the lines $(A'O_R)$ and $(B'O_R)$. The classical structure (CRt) is "opening" with the triangles rotating inward, the center of rotation O_R is the point A, and the edge of the structure E is thus defined as the point B. Building the N-order classical rotating-triangle structures (Fig. 8.b, c, and d), one uses the copy-rotation on the base structure around the center O_R and connects the revolute points A_{2n} to $A_{1(n+1)}$, with $n \in [1, N]$.

The reciprocal rotating-triangle (RRt) design has the triangles rotating outward (Fig. 8.e, f, and g), and the center of rotation is $O_R = B$. The two edges of the reciprocal structure are $E_1 = A_1$ and $E_2 = A_2$, the constructed edge E is the middle point of the segment $[A_1A_2]$ (Fig. 8.e). Building the N-order reciprocal rotating-triangle structure, one rotates the base structure around the center O_R and connects the edges of consecutive unit cells.

The N-order base rotating triangle structure has equal angles $\theta_1 = \theta_2 = \theta_N$, because the axis of symmetry $(A'B')$ splits the angles equally and the angle φ_N gives the value of θ_N as:

$$\theta_N = \frac{\varphi_N}{2} = \frac{360°}{2N} \tag{18}$$

The N-order rotating triangles structure is fully deployed when the triangles are fully open, i.e. when the final internal angle α_N is

$$\alpha_N = 180° - \varphi_N \tag{19}$$

Eq. (19) holds true for $N \geq 3$, indeed the case where $N = 2$ is fully deployed when $\alpha_N = 90°$. While the N-copy-rotations are resulting in auxetic designs, the case N = 2 showcases a meiotic structure both in the classical and reciprocal design.

An irregular variation of Rt with equilateral triangles possessing a diamond shape unit cell is illustrated in Appendix B, the tessellation

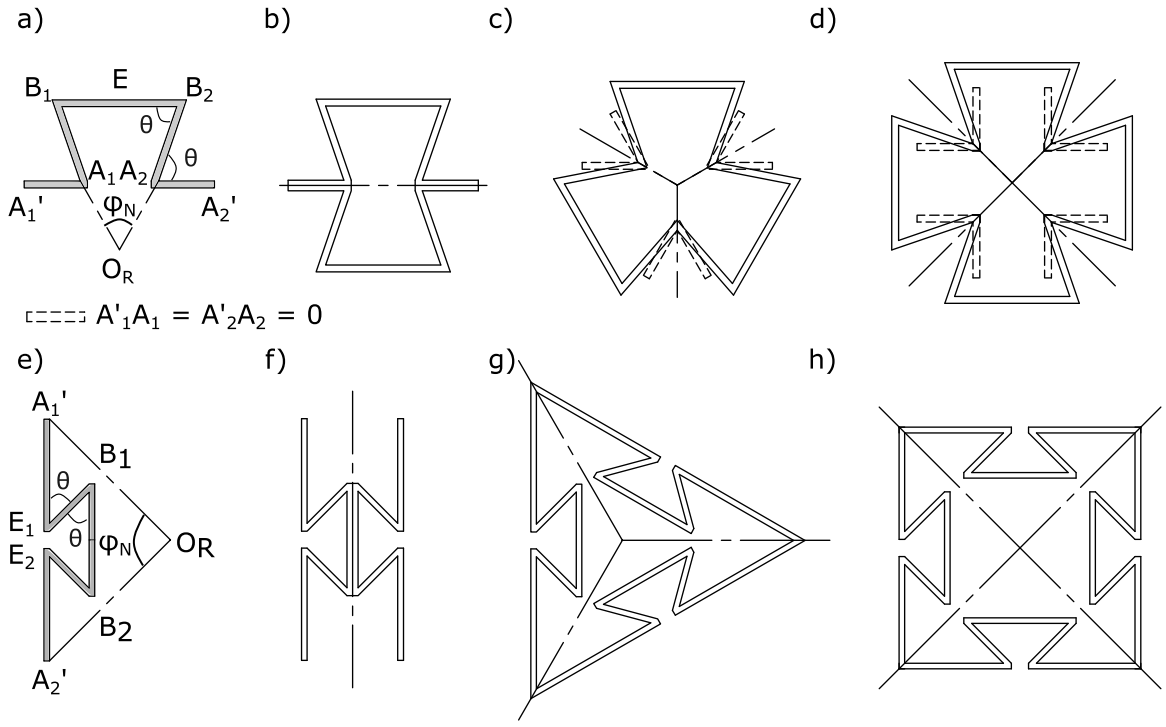

Fig. 7. Topological representation of the classical "puzzle tiles" auxetic achiral metamaterials, with (a) the construction of the center of rotation O_R, the representation of the undeployed (top) and deployed (bottom) case (b) 2CPt where $N = 2$, (c) 3CPt where $N = 3$, and (d) 4CPt where $N = 4$. Topological representation of the reciprocal "puzzle tiles" auxetic achiral metamaterials, with (e) the construction of the center of rotation O_R, the representation of the undeployed cases (f) 2RPt where $N = 2$, (g) 3RPt where $N = 3$, and (h) 4RPt where $N = 4$.

of the "Rt diamond" structure leads to the structure that is usually called "rotating rigid triangle" (Grima et al., 2011; Papadopoulou et al., 2017).

Other irregular structures can be created modifying the dimension of the Z structure, first, if the Z parameters are $a_1 = a_3$ and $a_2 \neq a_1\sqrt{2}$ the triangles are still right-triangles (for the base structure or $N = 2$) and not isosceles. The base structure thus becomes rectangular, in addition to the change of the shape, the modification of the parameters makes the structure chiral. Therefore, the structure can be copy-rotated as a chiral structure, but most importantly can be achiralised, the Appendix C illustrates this irregularity and details the calculation of the Poisson's ratio.

3.2. Building chiral structures

We present here how to create, from the Z structure (Fig. 5.a), the three chiral auxetic families, how to construct the center of rotation O_R and the edges E and apply the copy-rotation protocol for $N = 2, 3$, and 4.

3.2.1. Chiral auxetic honeycomb

Auxetic chiral "honeycomb" (Hc) metastructures (Lakes, 1991; Alderson et al., 2010; Pasini and Rafsanjani Abbasi, 2017; Mizzi and Spaggiari, 2022; Ren et al., 2023) are common chiral auxetic metamaterials. The center of rotation O_R is created from the triangle AO_RB, with the angle φ_N between the lines (AO_R) and (BO_R), and the edge E of the structure is located at the point A' (Fig. 9.a). Building the N-order honeycomb (Fig. 9.b, c, d), one uses the copy-rotation on the base structure around the center O_R and connects the points A_n to $B_{(n+1)}$, with $n \in [1, N]$. In the case $N = 2$ (Fig. 9.b), the angle $\varphi_2 = 180°$ position the point O_R at the center O, thus recreates the base chiral Z structure. For the copy-rotation of $N \geq 3$, the length of the beam BB_1 needs to be adapted for the point B_1 to be located in the beam AB_{n+1}, meaning that the central shape (triangle for $N = 3$, or square for $N = 4$) is over constrained and can thus be considered as a rigid body, as illustrated in Fig. 9.b,c. Thus the central rigid body can be rotated and only the legs $A_nA'_n$ are free to move.

The reciprocal design proposed for the achiral auxetic structures can also be applied to the chiral structures. The resulting structures are "anti-chiral", i.e. the structures are still chiral but mirrored from the classical chiral. The chiral and anti-chiral honeycomb structures are deployed when all the N copy-rotations are deployed to their maximum angle, i.e. when the angles θ_N are:

$$\theta_N = 180° - \frac{(180° - \varphi_N)}{2} = 90° + \frac{\varphi_N}{2} \tag{20}$$

A representation of the tessellated Hc3 and Hc4 structures topologies are represented undeployed and deployed in Fig. 9.d,e.

An irregular design, sometimes called "pattern p31 m" (Stavric and Wiltsche, 2019), is a variation of the $N = 3$ honeycomb design (Hc3). The axis of symmetry of the achiralised AHc3 is parallel and non colinear to one leg and is passing through one edge of an other of the three legs. The achiralised structure AHc3 is copy-rotated three times to form a structure that can be named "3AHc3 star" design, the structure and unit cell are depicted in Appendix B.

3.2.2. Chiral "missing-rib" auxetic

Chiral "missing-rib" (Gaspar et al., 2005; Clausen et al., 2015; Rafsanjani and Pasini, 2016; Jiang et al., 2019; Olvera et al., 2020; Attard et al., 2020; Zhu et al., 2022a; Zhang et al., 2022a; Zhu et al., 2022b) (Mr) topologies are quite common chiral metastructures that are close to the topology of the honeycombs. The center of rotation O_R is located at the point A' (or B′ depending on which orientation of chirality the users require) of the Z structure, with $\varphi_N = A_n\widehat{O_RA_{n+1}}$ the angle between two copies. As O_R is located at the position of the point A', the N-order missing-rib structures are created from a Z structure with the length of the beam $[BB'] = a_3 = 0$. The case $N = 2$ (Fig. 10.a) gives, as the honeycomb design, the topology of the base chiral Z structure. The copy-rotation Mr3 and Mr4 are presented in Fig. 10.b,c, the beams B_nA_n are connected rigidly at the center of rotation O_R.

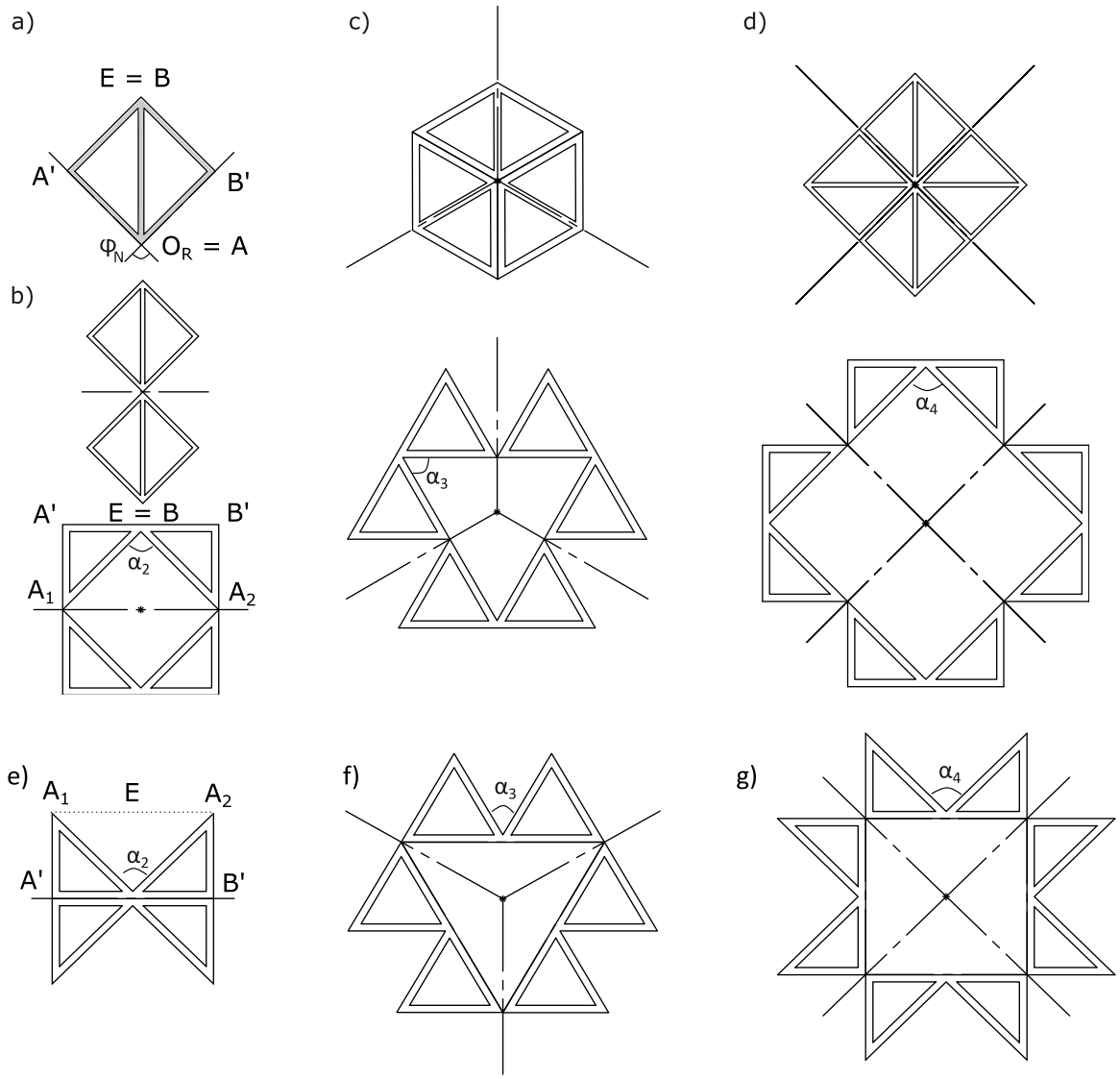

Fig. 8. The topological representation of the design of the regular achiral "rotating triangles" auxetic metamaterials, with (a) the construction of the center of rotation O_R and the representation of the undeployed (top) and deployed (bottom) of the classical designs for (b) 2CRt where $N = 2$, (c) 3CRt where $N = 3$, and (d) 4CRt where $N = 4$. The topological representation of the reciprocal designs for (e) 2RRt where $N = 2$, (f) 3RRt where $N = 3$, and (g) 4RRt where $N = 4$.

A representation of tessellated Mr3 and Mr4 structures are presented in Fig. 10.d,e to illustrate the auxeticity and behavior of the structures, which are fully deployed when the angles $\theta_N = 180°$, in this configuration, all legs of the Mr structures are extended to their maximum.

Oppositely to the achiral connected stars, for the even N cases, the center cross-like rigid body does not decouple the branches because of the chiral property of the structure input a natural twist around the point O_R when two opposite edges are stretched or compressed.

3.2.3. Chiral auxetic closed-geometry

We present here novel chiral "closed-geometry" (Cg) auxetic metastructure, represented in Fig. 11. The center of rotation O_R is created from the triangle $(A'O_RB')$, with the angle φ_N between the lines $(A'O_R)$ and $(B'O_R)$, and the edge E of the structure is located at the projection of O_R in the beam A′A (or B′B if the structure is chosen chiral or anti-chiral).

As for the honeycomb and missing-rib, the 2 copy-rotation is not changing the topology of the Z. Building the N-order closed-geometry (Fig. 11.b, c), one uses the copy-rotation on the base structure around the center O_R and connects rigidly the points A'_n to $B'_{(n+1)}$, with $n \in [1, N]$.

A representation of the tessellation of Cg3 and Cg4 are depicted in Fig. 5.d,e the structures are deployed when all the N structures are deployed to their maximum, i.e. when the angles $\theta = 90°$. One could perceived the Closed-geometry topology as a chiral variation of the connected stars.

3.3. Building complex higher-order auxetic structures

The copy-rotation process can be continued for higher order N for the six auxetic families presented above and can, theoretically continue to infinity. In addition, we present here how the N-order auxetic structures can be used as a base to create more complex structures via both the copy-rotation and the achiralisation processes. Such higher-order design can generate hierarchical auxetic planar metamaterials (Gatt et al., 2015a; Hamzehei et al., 2018).

3.3.1. Higher order copy-rotation of auxetic structures

The copy-rotation process can be applied using N-order auxetic structures as a rotated structure. Most of the structures presented above

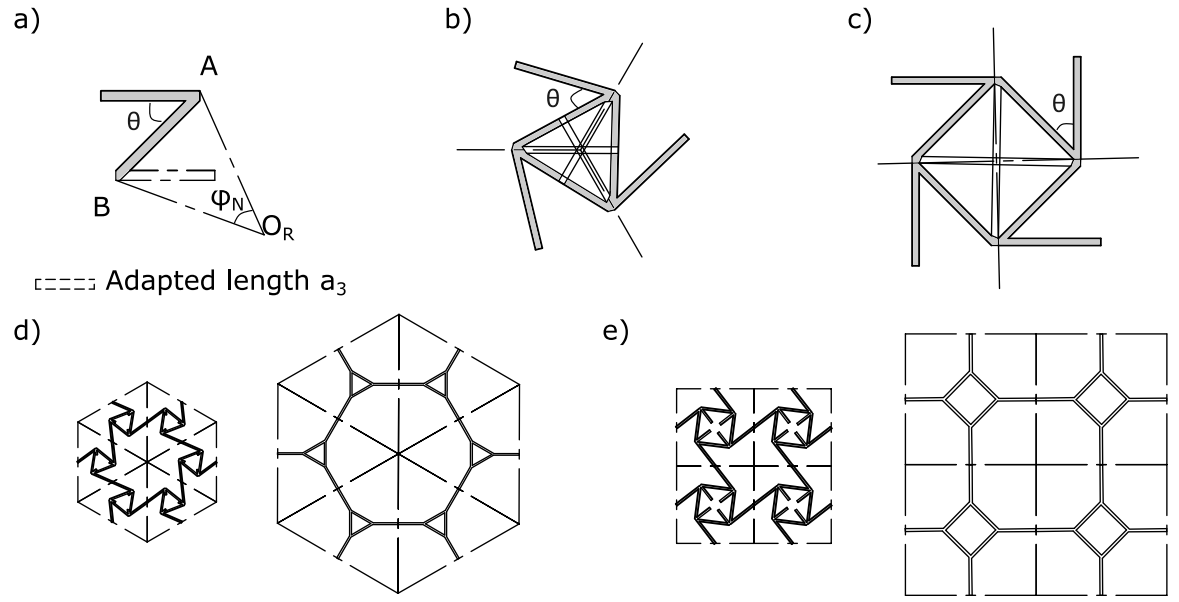

Fig. 9. Geometrical design of the chiral "honeycomb" auxetic metamaterials, with (a) the construction of the center of rotation O_R, the representation of the undeployed (top) and deployed (bottom) case (b) Hc3 where $N = 3$, and (c) Hc4 where $N = 4$. Representation of the undeployed (left) and deployed (right) tiling of unit cells of (d) Hc3 and, (e) Hc4.

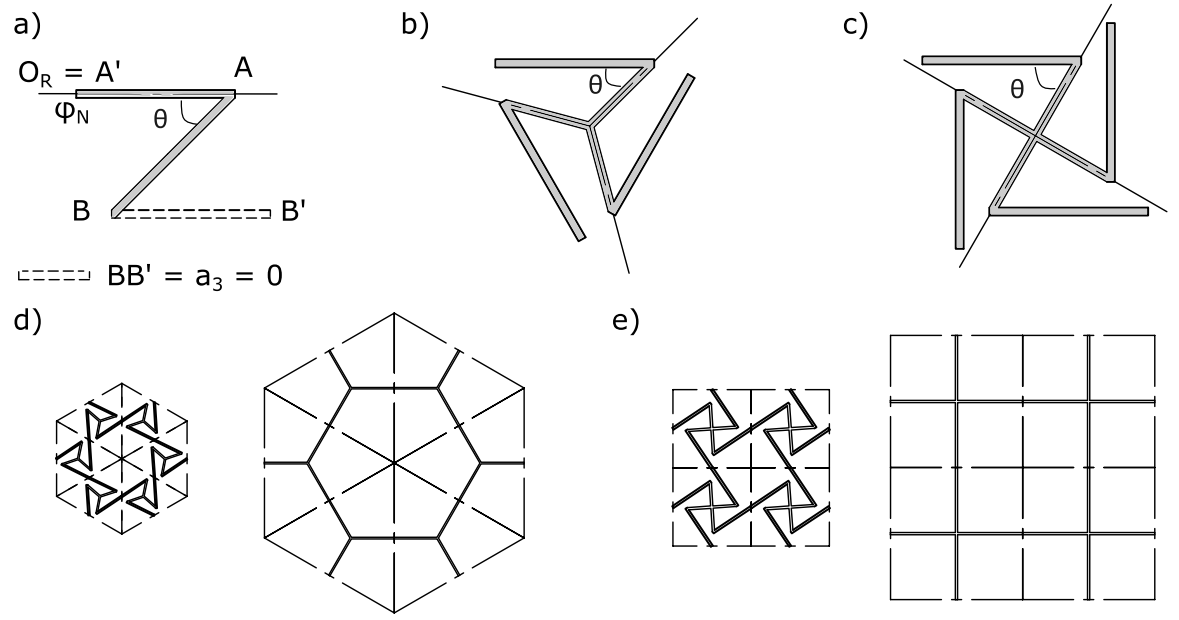

Fig. 10. Topological representation of the design of the missing-rib auxetic chiral metamaterials, with (a) the construction of the center of rotation O_R, the representation of the undeployed (top) and deployed (bottom) case (b) Mr3 where $N = 3$, and (c) Mr4 where $N = 4$. Representation of the undeployed (left) and deployed (right) tiling of unit cells of (d) Mr3 and, (e) Mr4.

can be copy rotated to create higher order auxetic structures, the design protocol is the same as previously, the center of rotation O_R is defined this time by the triangle $(E_1O_RE_2)$, formed by two edges of the chosen structure E_1 and E_2. The angle φ_M, with M the number of order of copy-rotation of the N order copy-rotated structures, is defined by the intersection of the lines (E_1O_R) and (E_2O_R), the M structures are rotated around O_R. The angle φ_M defined the possible regular structures that can be produced. If φ_M is a divisor of 360°, with k_0 is an integer, such as

$$360 = k_0 \times \varphi_M \tag{21}$$

and $k_1, k_2, \ldots k_n$ are divisor of k_0, such as,

$$360 = k_1 \times k_2 \times \cdots \times k_n \times \varphi_M \tag{22}$$

then the base structure can be copy-rotated k_0 times, or k_1 times, or k_2 times, ...or k_n times in a regular manner. The case where $k_n = 1$ produces the initial structure and, $k_n = 2$ tessellates the initial structure, therefore these cases can be avoided. If the structure is copy-rotated a number k_m times with k_m not a divisor of 360° the structure created is irregular and its geometry needs to be adapted to be tessellated.

Examples of regular and irregular structures are given in (Fig. 12.a,b,c,d,e) for the honeycomb chiral structures and in

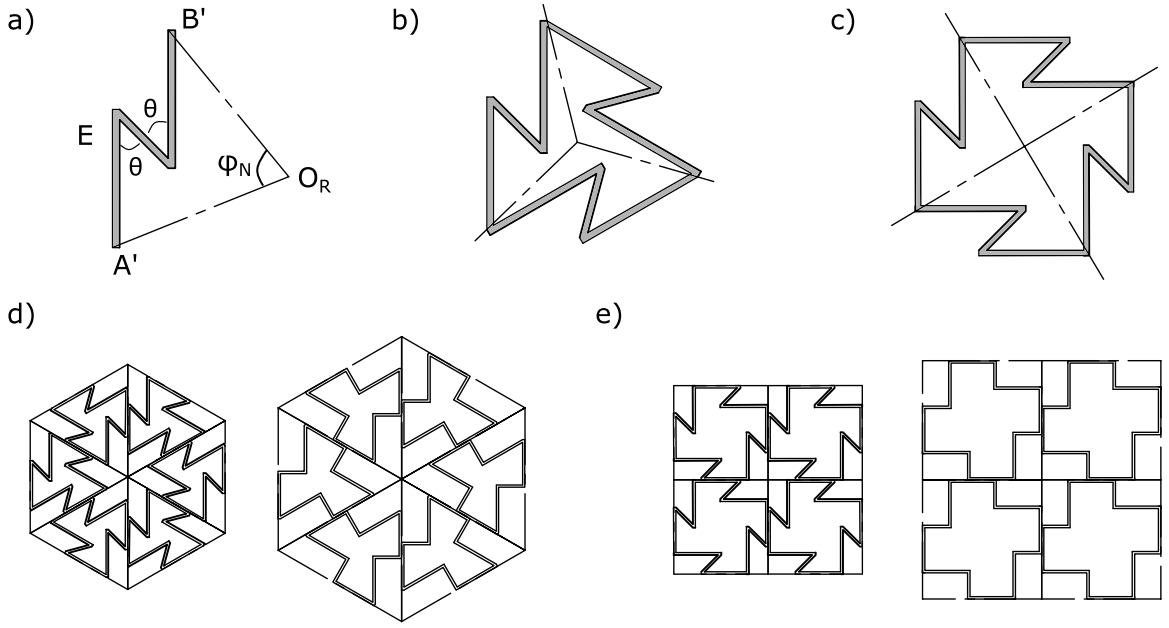

Fig. 11. Topological representation of the design of the regular chiral "closed geometries" auxetic metamaterials, with (a) the construction of the center of rotation O_R, the representation of the case where (b) Cg3 where $N = 3$, and (c) Cg4 where $N = 4$. Representation of the undeployed (left) and deployed (right) tiling of unit cells of (d) Cg3 and, (e) Cg4.

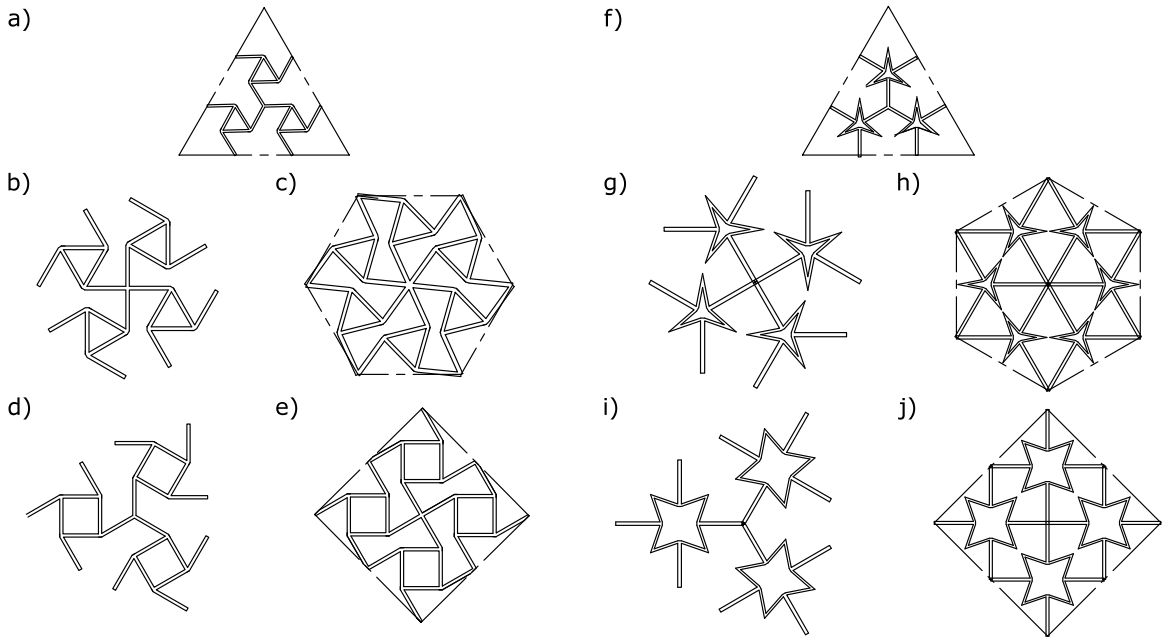

Fig. 12. The representation of some higher order copy-rotation, of the honeycomb (Hc) design with, the regular design (a) $N = 3$ and $M = 3$ (Hc3.3), the irregular design (b) $N = 3$ and $M = 4$ (Hc3.4), the regular design (c) $N = 3$ and $M = 6$ (Hc3.6), the irregular design (d) $N = 4$ and $M = 3$ (Hc4.3), and the regular design (e) $N = 4$ and $M = 4$ (Hc4.4). The representation of some higher order copy-rotation, of the reciprocal connected stars (CCs) design with, the regular design (f) $N = 3$ and $M = 3$ (3.3CCs), the irregular design (g) $N = 3$ and $M = 4$ (4.3CCs), the regular design (h) $N = 3$ and $M = 6$ (6.3CCs), the irregular design (i) $N = 4$ and $M = 3$ (3.4CCs), and the regular design (j) $N = 4$ and $M = 4$ (4.4CCs).

(Fig. 12.f,g,h,i,j) for the achiral reciprocal connected stars design. The order of the new structures can be defined as an $M.N$ order, see Section 2.3 for the details of the naming protocol.

3.3.2. Achiralisation of higher order chiral structures

The process of achiralisation can be applied to design achiral structures from N orders, or more complex, chiral structures. The chiral structures presented above can be used in the achiralisation process, by joining two enantiomorphs together, forming an achiralised structure. The achiralised metastructures can be copy-rotated once more, two regular options of design are possible, having a classical or reciprocal design type. A classical design possesses the center of rotation O_R on the side where the virtual edge E_C is the closest to the edge points E_n, oppositely the reciprocal design possesses the points E_n the furthest to E_R, as depicted in Fig. 13.a,b,c,d. The achiralised N order structures can be copy-rotated M times to form higher-order achiral auxetic structure, by defining a center of rotation O_R and an edge point E following the same design protocol. Examples of these achiral higher-order classical and reciprocal metastructures are presented in Fig. 13

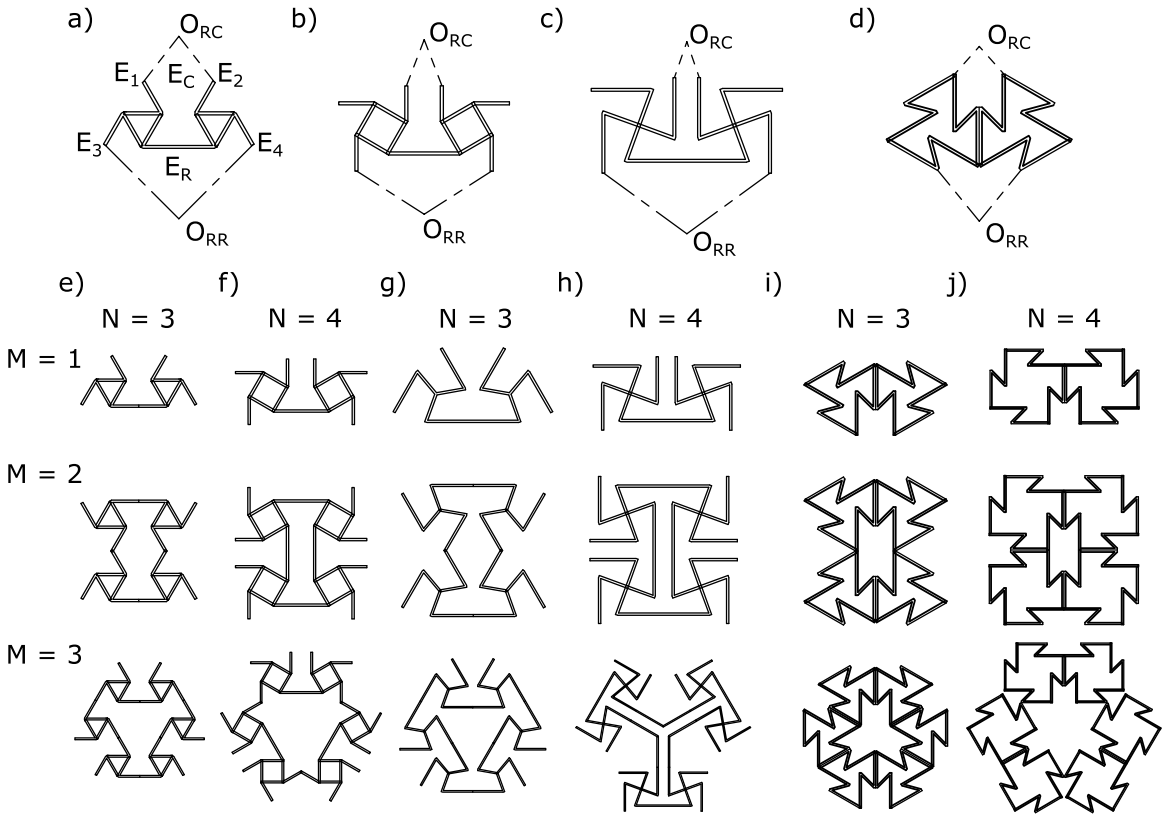

Fig. 13. The achiralisation and representation of the classical O_{RC} and reciprocal O_{RR} center of rotation of (a) AHc3, (b) AHc4, (c) AMr4, and (d) ACg3. Topological representation of the achiralised structures of (e) the classical copy-rotation of AHc3 with 2CAHc3 and 3CAHc3, (f) the reciprocal copy-rotation of AHc4 with 2RAHc4 (Lipton et al., 2018; Broeren et al., 2020; Ren et al., 2023) and 3RAHc4, (g) the classical copy-rotation of AMr3 with 2CAMr3 and 3CAMr3, (h) the classical copy-rotation of AMr4 with 2CAMr4 (Li et al., 2018) and 3CAMr4, (i) the classical copy-rotation of ACg3 with 2CACg3 and 3CACg3, (j) the classical copy-rotation of ACg4 with 2CACg4 and 3CACg4.

for the honeycomb, missing-rib, and closed geometry chiral structures for $M = 3, 4$ and $N = 2, 3$.

3.3.3. Hierarchical and fractal auxetic metamaterial structures

Hierarchical structures are formed by assembling structural elements, which themselves possess a nested structure (Gatt et al., 2015a; Li et al., 2021; Shen et al., 2021). Hierarchical auxetic structures can be derived from chiral structures that undergo at least two levels of copy-rotation, followed by an achiralisation process, and finally another copy-rotation step. For example, Hc4 is subjected to four copy-rotations, resulting in Hc4.4, then achiralized to AHc4.4, and finally copy-rotated two times in the reciprocal design to obtain 2RAHc4.4, as depicted in Appendix F. The structure 2CAHc3.4 (Hamzehei et al., 2018) has been proposed as a hierarchical auxetic metamaterial for the investigation of significant compressive deformation.

Fractal structures are self-replicating patterns found at all scales, and are abundant in both natural and engineering contexts (Mandelbrot, 1983; Wang et al., 2022). These proposed auxetic designs can serve as fundamental building blocks for creating larger-scale structures with the same design.

Both hierarchical and fractal auxetic metamaterials offer intriguing possibilities for controlling and programming the deformation behavior of a structure.

3.4. Tessellation of auxetic metamaterials

Metamaterials can be seen as artificial crystal structures (Frenzel et al., 2017; Fernandez-Corbaton et al., 2019) and their main constituents can be, thus, identified as unit cells that repeat in a lattice structure and be tessellated in the plane. We are going to consider the structures by their contour, a repeatable geometrical object, that we call the auxetic unit cell (UC). We propose, in the following sections, a method to design the unit cells of the above-presented auxetic structures, a way to tessellate identical unit cells with the Wigner–Seitz tessellation and, presented in Appendix E a way to tessellate different unit cells together following an Archimedean and Laves tiling.

3.4.1. The voronoi decomposition

Through the achiralisation and the copy-rotation design protocols, we have been presenting chiral and achiral auxetic N-order structures. To conserve the auxeticity order, the unit cell of an N-order auxetic structure will be defined as an N-face polygon. The unit cells are built from a Voronoi decomposition of the auxetic structures (Fig. 14), the protocol for the construction of the unit cell is the following:

Step 1. The center of rotation O_R is a vertex of the unit cell,
Step 2. For each sector, the segment $[O_R E]$, with E the edge point of the sector, is perpendicular to the face $[F]$ of the sector,
Step 3. The edge E, or equivalent edge, is the center point of the segment $[F]$,
Step 4. The angle α between two faces of the unit cell is

$$\begin{aligned} \alpha &= 360° - 90° - 90° - \varphi_N \\ &= 180° - \varphi_N \end{aligned} \tag{23}$$

In the case of $N = 2$, the two faces produced by this protocol are parallel, one needs to complete the drawing of the unit cell drawing two lines that passes through the two points used to build the center of rotation O_R (e.g. the creation of the unit cell of the case $N = 2$ of the connected stars Fig. 14.a). The Fig. 14.b,c,d,e represents examples of unit cells design protocol for low order auxetics. The Fig. 14.f represents the unit cell of the 4.4CCs classical connected star design. The Fig. 14.g give an example of the unit cell of the 3CACg3 achiralised

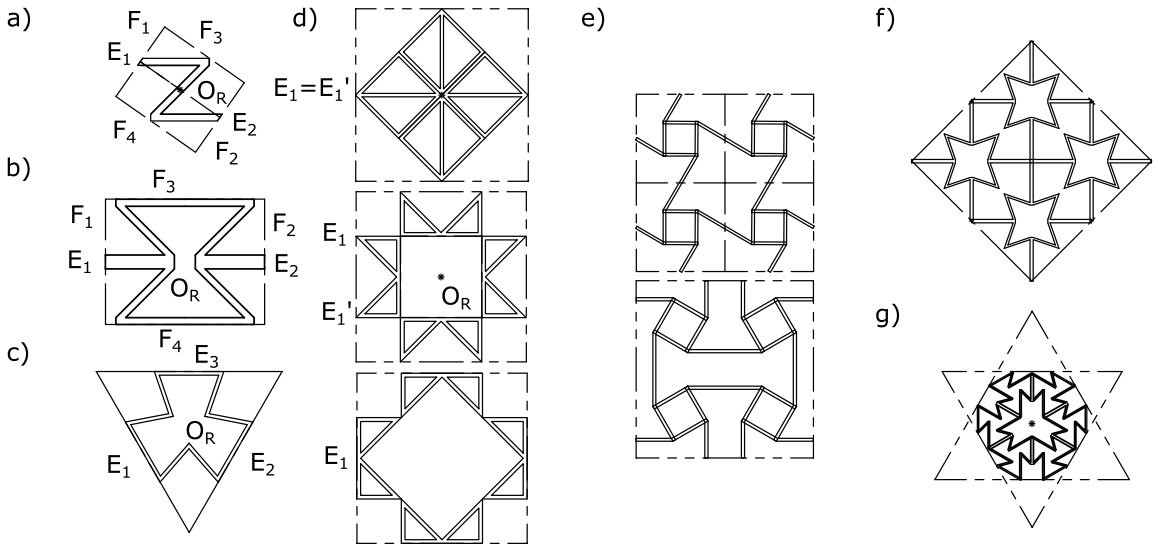

Fig. 14. Representation of the Voronoi decomposition for the creation of the unit cells of (a) the base Z structure, (b) bow tie, $N = 2$ connected star (2CCs), (c) the classical puzzle tiles with $N = 3$ (3CPt), (d) the undeployed and deployed version of the $N = 4$ classical (4CRt) and reciprocal (4RRt) rotating triangles, (e) the chiral honeycomb with $N = 4$ (Hc4) and it is achiralised higher order (2AHc4), (f) the higher order copy rotated classical connected stars (4.4CCs) and, (g) the higher order achiralised closed geometry copy rotated three times (3CACg3).

closed geometry, two triangular unit cell possibilities exist from the design protocol, however one is not separable form the other. In this case, the union of the two UC can be taken, forming an hexagon, to use it as a unit cell, one needs to design the structure to be a regular hexagon and be sure that the edge points can connect to the following unit cell.

3.4.2. The Wigner–Seitz tessellation, or regular tiling

Auxetic metastructures are formed by a repetition of a unique auxetic unit cell that is repeated in space (Kolken and Zadpoor, 2017; Czajkowski et al., 2022).

The Voronoi decomposition and the tessellation of a unique and minimal unit cell have been proposed as the Wigner–Seitz (WS) cell. The WS cell is a primitive cell that possesses a discrete translational symmetry, i.e. the repetition of the WS cell follows a translation $\vec{T}$ following two unit vectors $\vec{a_1}$ and $\vec{a_2}$

$$\vec{T} = u_1\vec{a_1} + u_2\vec{a_2} \tag{24}$$

with u_1 and u_2 integers. Thus the WS cell is able to describe the repetition of the same unit cell in space, in 2D, they are represented by two types of parallelograms (presented in Appendix E) that are either lozenges ($N = 2, 4$) (rectangles and squares) or hexagons ($N = 6$). Triangular unit cells ($N = 3$) are to be joined to a second triangular cell to form a lozenge to be a tessellable WS cell. The Wigner–Seitz tessellation gives the possibility to tessellate similar unit cells, however, it is limited to a few geometrical shapes. A more complete lattice definition uses the Archimedean or semiregular tiling of polygons. Archimedean tiling or plane-vertex tiling (also semiregular tiling) uses regular convex polygons that can form 21 plane-vertex tilings (Golomb et al., 1988). The tessellation possibilities offered by the plane vertex tiling, also called archimedean or Laves tiling are detailed in Appendix E.

3.5. A general metric for auxetics, surface strain, bulk modulus and compressibility

The design method produces an infinite amount of topologies. For certain instances, the calculation of Poisson's ratio can be challenging when structures do not possess a natural x/y orientation. In this regard, the unit cells of structures can be defined for tessellating the structures and exploiting the copy-rotation symmetry that enables full definition in the N direction of auxeticity. By considering the unit cell as a whole auxetic element, surface strain ε_S can be used by applying it directly to the unit cell.

$$\varepsilon_S = \frac{S_F - S_I}{S_I} \tag{25}$$

with S_I and S_F the initial and final surface area of the unit cell. Unlike the Poisson's ratio, which is limited to directionality, i.e., dimensions x and y, the surface strain is directionless and considers all the N directions of an N-order auxetic metamaterial. The calculation of the surface strain uses the surface area of one sector (S_{I_N}, S_{F_N}) multiplied by the number N of sectors.

$$\begin{aligned} S_I &= N \times S_{I_N} \\ S_F &= N \times S_{F_N} \end{aligned} \tag{26}$$

To calculate the surface area of a sector, one needs to consider the inner and outer borders of the repeated element. For instance, the calculation of the surface strain ε_S and the Poisson's ratio ν of the simple case of the bow-tie structure (2CCs) can be derived (Fig. 15.a). The initial length and height of 2CCs can be written as

$$L_I = 2(a_1 + a_3 - a_2\cos(\theta)) \tag{27}$$

$$H_I = 2a_2\sin(\theta) \tag{28}$$

For an ideal deformation, when stretched, the structure deploys and thus only the angle θ changes. The angle can be considered to grow with a variation δ, therefore going from θ to $\theta+\delta$ (Fig. 15.b). Thus, the final length and height are

$$L_F = 2(a_1 + a_3 - a_2\cos(\theta + \delta)) \tag{29}$$

$$H_F = 2a_2\sin(\theta + \delta) \tag{30}$$

The directional strains (ε_L and ε_H), the Poisson's ratio ν and the surface strain (Eq. (25)) can be thus formulated. The structure 2CCs is a topology close to 4RCs and therefore the length and height can be found following the same process, while taking into account the anepirretic behavior of the structure.

For N copy-rotation structures, the calculation of the surface strain can be simplified, considering each sector independently. For instance the surface strain of the family of the connected stars (Cs) designs can be simplified by analyzing the surface of the copy-rotated element (Fig. 15.c.d). The sector can be split into two right triangles, right in E,

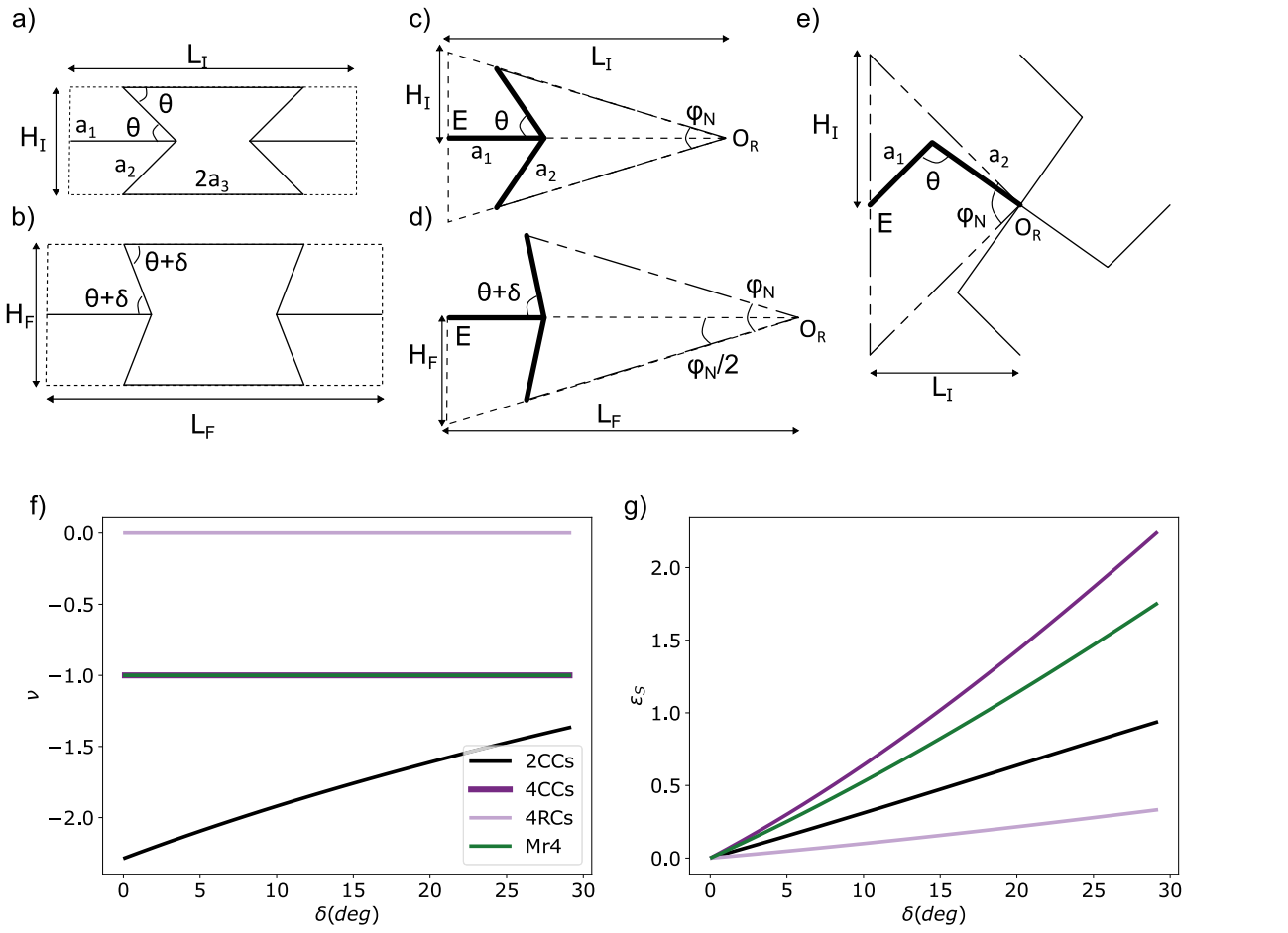

Fig. 15. Representation of (a) the structure 2CCs (Bowtie) undeformed, (b) 2CCs deformed at the angle $\theta + \delta$. The details of the surface area of one sector of the Cs family with (c) the undeformed, and (d) deformed structure. Representation of (e) the Mr4 chiral structure for the calculation of the surface area. Evolution, for the structures 2CCs, 4CCs, 4RCs and Mr4, of (f) the Poisson's ratio ν, and (g) the surface strain ε_S.

of angle $\frac{\varphi_N}{2}$, enabling trigonometry to be used to calculate the surface area of the right triangle, and therefore, the isosceles triangle. The initial length is written as a function of θ and N as

$$L_I(\theta, N) = a_1 - a_2\cos(\theta) + \frac{a_2\sin(\theta)}{\tan\left(\frac{\varphi_N}{2}\right)} \tag{31}$$

and the initial height as

$$H_I(\theta, N) = L_I(\theta, N)\tan\left(\frac{\varphi_N}{2}\right) \tag{32}$$

The surface area of a unit cell S_I is therefore determined by the number N of copy-rotations as stated in Eq. (26).

$$S_I(\theta, N) = N H_I(\theta, N) L_I(\theta, N) \tag{33}$$

As φ_N is fixed by design, only θ changes with δ. The case of 4CCs is using four copy-rotations and thus the total length and height can be derived as well as the Poisson's ratio. The parametrization of the structure Mr4 is presented in Fig. 15.e where the length of one sector is calculated as

$$L(\theta) = \sqrt{a_1^2 + a_2^2 - 2a_1a_2\cos(\theta)} \tag{34}$$

and the height is

$$H(\theta) = L(\theta)\tan\left(\frac{\varphi_N}{2}\right) \tag{35}$$

The evolution of Poisson's ratio and surface strain are plotted in Fig. 15.f.g with the evolution of δ for an initial angle $\theta = 40°$ for the structures 2CCs, 4CCs and 4RCs and Mr4. The calculations of the sectors' parameters for Mr4 and 4RCs (as for all other structures) are based on the same approach. The Poisson's ratio for 4CCs and Mr4 as for many 4-copy-rotations is -1, this is explained by the fact that all sectors behave the same and a Poisson's ratio in x and y direction can be calculated (and projected in the xy base).

The surface strain, by its independence from any axis, gives more general information on the behavior of the auxetic structures. Indeed, the surface strain ε_S gives the information about the surface bulk modulus K_S of the auxetic structure

$$K_S = -\frac{\sigma_S}{\varepsilon_S} \tag{36}$$

with σ_S the surface stress applied to the edge of the unit cell. One can define the surface compressibility β_S, the inverse of the bulk modulus

$$\beta_S = \frac{1}{K_S} \tag{37}$$

Auxetic metamaterials increase in surface area $\varepsilon_S > 0$ when stretched, i.e. with a negative pressure $\sigma < 0$ (resp decrease $\varepsilon_S < 0$ when compressed, with a positive pressure $\sigma > 0$), therefore the surface bulk modulus K_S is positive for auxetic metamaterials and therefore the compressibility always positive and can be very large if the surface strain ε_S is very large too. Highly positive compressible structures were named "supercompressible" metamaterials (Bessa et al., 2019; Houlder and Bessa, 2019; Liu et al., 2020).

4. Discussion

The design protocol proposed using the achiralisation and copy-rotation topological transformations appears to offer infinite possibilities for creating auxetic structures. The creation of some structures

require a modification of the length of some beams and of the angles, this particularity enables the creation of an infinite amount of topologies. Many of these structures, particularly those with higher orders, cannot be tessellated with regular tiling. We anticipate that such complex structures may be useful for specific applications due to their designed Poisson's ratio, compressibility or deformation behavior.

While we have primarily focused on regular topological designs, we note that introducing irregularities can lead to even more unique and specialized auxetic structures. Such irregularities can be introduced geometrically through mismatches in lengths and angles, or in the copy-rotation protocol itself by modifying each of the N repeated entities to behave in a unique manner in each of the N directions. We have shown that the higher order copy-rotation protocol, with $N.M$ copy-rotations when $N \neq M$, can also introduce irregularities, although modifications to the structure may be required to create a complete unit cell.

Naming conventions for irregular structures may need to be adapted to reflect classes of irregularities. For example, the addition of a lowercase I or adding a detail after the regular name (for instance Rt diamond rotating triangle design, presented in Appendix B) could signify an irregularity in some cases, but might not be required for structures such as 3.4.RCs (Fig. 12.i), which are irregular due to the "3.4" copy-rotation mismatch.

Tessellating auxetic structures from a Wigner–Seitz or Archimedean tiling appears to be well-defined for structures within the same scaling range. Modifications to the tiling can be introduced through a hierarchy effect, such as dividing a geometrical object into sub-objects that do not change the outer shape of the unit cell but introduce additional internal complexity. Irregularities in the tiling of geometrical shapes could be used to define different auxetic regions within a planar surface.

The presented calculations take into account a perfect topology, with rigid beams and revolute joints, the embodiment analysis of the structures would necessarily not be ideal and deflection of the beams, and spring stiffness of the joints need to be added.

We did not find any 2D auxetic metamaterial that could not be designed following our proposed design method, however, we did not prove yet our method can generate all possible auxetic structures.

We considered the Z structure only in a part of its range of motion from the initial configuration to the maximum auxeticity. It would be interesting to consider the other part of its range of motion leading to meiotic behavior (Positive Poisson's ratio). It is likely that a similar approach could be developed which is left for future study.

5. Conclusion

In summary, we have presented a comprehensive study on the design and classification of auxetic structures. Our approach involves the use of chiral and achiral elements, along with geometrical symmetries, to create a variety of auxetic structures with positive, null, or negative Poisson's ratios. We have proposed a design method that enables the recreation of existing and the creation of novel auxetic structures, with the flexibility to accommodate minor irregularities. Additionally, we have introduced a naming protocol for the structures, which allows for easy identification of their type, chirality, and geometrical complexity. Our designs can be tessellated in the plane, and we have provided a detailed construction process for the unit cells and described how to tessellate 2D auxetic structures. Finally, we have proposed using the surface strain of the unit cell as a general metric for auxetic structures, which relates directly to the bulk modulus and compressibility of the metamaterial. Overall, our findings provide a valuable contribution to the field of auxetics and can serve as a basis for the design and fabrication of new auxetic metamaterials with unique mechanical properties.

CRediT authorship contribution statement

Pierre Roberjot: Conceptualization, Formal analysis, Writing – original draft, Writing – review & editing. **Just L. Herder:** Methodology, Supervision, Validation.

Declaration of competing interest

The authors declare that they have no known competing financial interests or personal relationships that could have appeared to influence the work reported in this paper.

Data availability

No data was used for the research described in the article.

Acknowledgment

This publication is part of the project Mechanical Metamaterials for Compact Motion Systems (MECOMOS), project number 18940 of the Open Technology Program financed by the Dutch Research Council (NWO).

Appendix A. Puzzle tiles arrowhead design

See Fig. A.16.

Appendix B. Rt diamond

See Fig. B.17.

Appendix C. Rt irregular

The irregular Rt_I structure is presented in Fig. C.18.a, the irregularities are making the structure chiral and therefore, can be copy-rotated as a chiral structure, Rt_I4 is illustrated in Fig. C.18.d. As the Rt_I is chiral it can be achiralised and copy-rotated, the case $2CARt_I2$ is illustrated in Fig. C.18.b.c. The base structure is composed of two achiralised Rt_I, where the points B_1, B_2, A_2 and A_4 are hinges, and the triangle B_1B_2B is rigid. The unit cell of the structure is rectangular and therefore the value of the Poisson's ratio might differ from square unit cells. To simplify the writing of the Poisson's ratio one could write $a = a_1 = a_3$, and $b = a'_1 = a'_3$, with $b > a$. The initial parameters of length and height can be calculated as

$$L_I = 2b \tag{C.1}$$

and

$$H_I = 2a \tag{C.2}$$

The intermediate values can be written as

$$L = 2(b + a\cos(\alpha)) \tag{C.3}$$

and

$$H = 2(a\sin(\alpha) + b\cos(\alpha)) \tag{C.4}$$

with the angle $\alpha = \widehat{A_1B_1A'_1} \in [90°, 0°]$ with the point A'_1 the projection of the point A_1 on the line (B_1B_2). The final parameters are

$$L_F = 2(a + b) \tag{C.5}$$

and

$$H_F = 2b \tag{C.6}$$

Therefore, the strain and Poisson's ratio can be derived

$$\varepsilon_L = \frac{2(a+b)}{2b} - 1 = \frac{a+b}{b} - 1 = \frac{a}{b} \tag{C.7}$$

and

$$\varepsilon_H = \frac{2b}{2a} - 1 = \frac{b}{a} - 1 \tag{C.8}$$

Thus the Poisson's ratio between the initial and final state is

$$\nu = -\frac{\varepsilon_H}{\varepsilon_L} = -\left(\frac{b}{a} - 1\right)\frac{b}{a} = -\frac{b^2 - ab}{a^2} \tag{C.9}$$

The value of the Poisson's ratio is different from -1 between the initial ad final state, it might exists an intermediate value of $\nu = -1$, however, for this structure the Poisson's ratio ($\nu(a, b)$) can be tuned with the values of a and b. For instance $\nu(2, 1) = -2$ and $\nu(3, 1) = -6$.

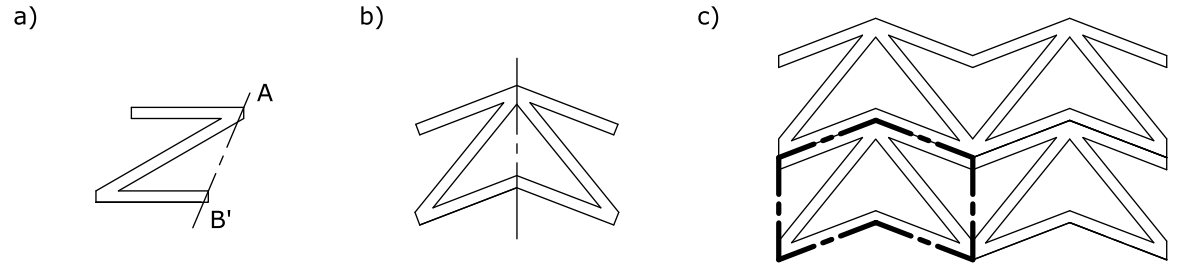

Fig. A.16. An irregular variation of the $N = 2$ puzzle tiles, usually called the "arrowhead" auxetic design (Larsen et al., 1997; Boopathi et al., 2020; Gao et al., 2020). (a) drawing of the axis of symmetry passing through the points A and B', (b) representation of "Pt arrowhead" and, (c) the representation of the unit cell in a stack of four.

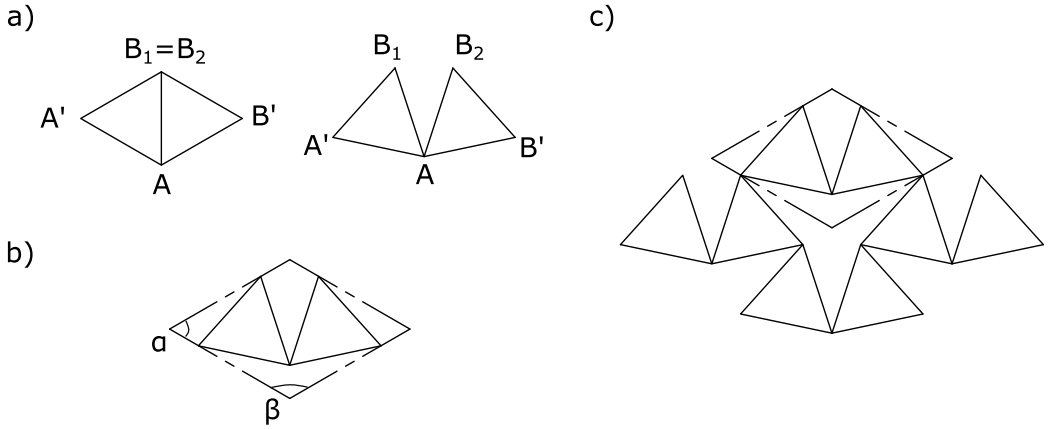

Fig. B.17. The particular case "Rt diamond" of the rotating triangle family (Grima et al., 2011; Papadopoulou et al., 2017). Rt diamond is a variation of the Rt achiral base, where the two rotating triangles are equilateral, where $\widehat{A'AB'} = 120°$, represented in (a) the base Rt diamond undeformed and deformed, (b) shows the unit cell design passing by the points A', B', B_1 and B_2 with the angles $\alpha = 60°$ and $\beta = 120°$. (c) Representation of the tessellation of four unit cells of Rt diamond.

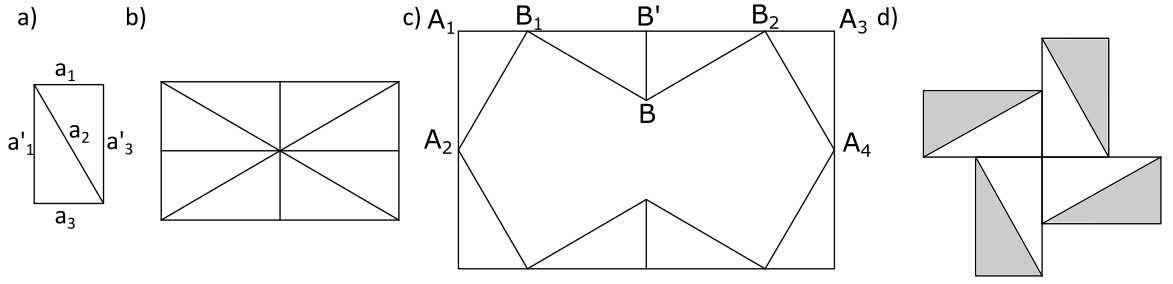

Fig. C.18. Representation of (a) the irregular chiral Rt structure (Rt_I) case where $a_1 = a_3 \neq a'_1 = a'_3$, and (b) the achiralised (ARt_I2) and copy-rotated two times ($2CARt_I2$) undeployed and (c) deployed structures. Representation (d) of the copy-rotation of Rt_I4, the irregular structure presents a topology close to Mr4, where the triangles in gray are rotating and the white ones are fixed.

Appendix D. Honeycomb 3AHc3 star design

See Fig. D.19.

Appendix E. Archimedean and Laves semiregular tiling

The Wigner–Seitz tessellation gives the possibility to tessellate similar unit cells, however, it is limited to a few geometrical shapes. A more complete lattice definition uses the Archimedean or semiregular tiling of polygons. Archimedean tiling or plane-vertex tiling (also semiregular tiling) uses regular convex polygons that can form 21 plane-vertex tilings (Fig. E.20) (Golomb et al., 1988).

The Archimedean tiling gives an understanding of how to tessellate the unit cells together, in addition, it is possible to view the tiling not from the geometry of the unit cell but from the connection of the vertexes, or how to connect the center of rotations O_R of the auxetic metamaterials by their edge points E. This type of tiling is called "Dual" or "Laves" tiling. The Laves tiles are called "planigons", convex polygons that connect the vertexes of the neighbor unit cells, each side of a planigon is normal to the line formed by two vertexes. Planigon

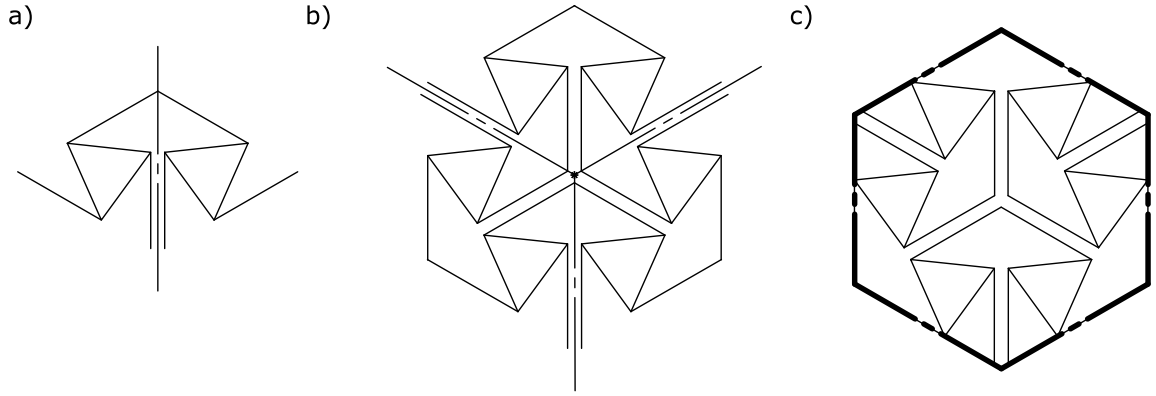

Fig. D.19. The particular case "AHc3 star" design is also called "pattern p31 m" (Stavric and Wiltsche, 2019). AHc3 star is a variation of the $N = 3$ honeycomb design Hc3, where (a) the axis of symmetry of AHc3 is parallel to one leg and is passing through one edge of an other of the three legs. (b) The achiralised structure AHc3 is copy-rotated three times to form a structure that can be named "3AHc3 star" design, in (c) is a drawing of the unit cell.

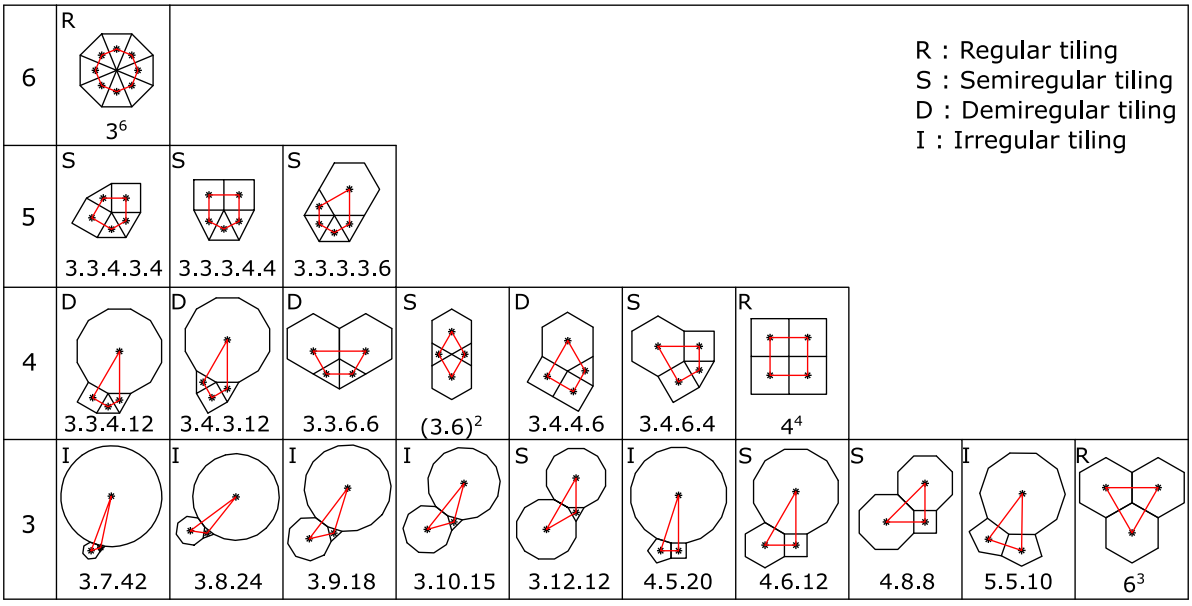

Fig. E.20. Archimedean tiling of the unit cells and Laves tiling with the construction of the planigons (Golomb et al., 1988).

notation uses a naming protocol, the letter V for vertex is followed by the geometrical orders of the planigons forming the tiling pattern that fill the plane, as an example $V4.4.4.4$ or $V4^4$ is the notation for the planigon connecting 4 square (4) unit cells, also $V4.8.8$ or $V4.8^2$ is the notation for the planigon connecting a square (4) and two octagons (8).

One can distinguish the 21 planigons in four families,

(i) 3 regular planigons are the equilateral triangles, squares, and regular hexagons;
(ii) 8 semiregular planigons such as triangles, quadrilaterals, and pentagons;
(iii) 4 "demiregular" planigons, they can only fill the plane combining other planigons;
(iv) 6 irregular planigons that can fill the plane only by combining with irregular polygons.

Planigons are tiled edge-to-edge as the angles are divisors of 360° and connect the vertexes together.

The Archimedean and Laves tiling give the possibility to extend the tessellation to more complex lattices through the process of complex Euclidean tiling and geometrical fractalization (Gomez-Jauregui et al., 2021).

Appendix F. Illustration of the naming protocol

See Fig. F.21.

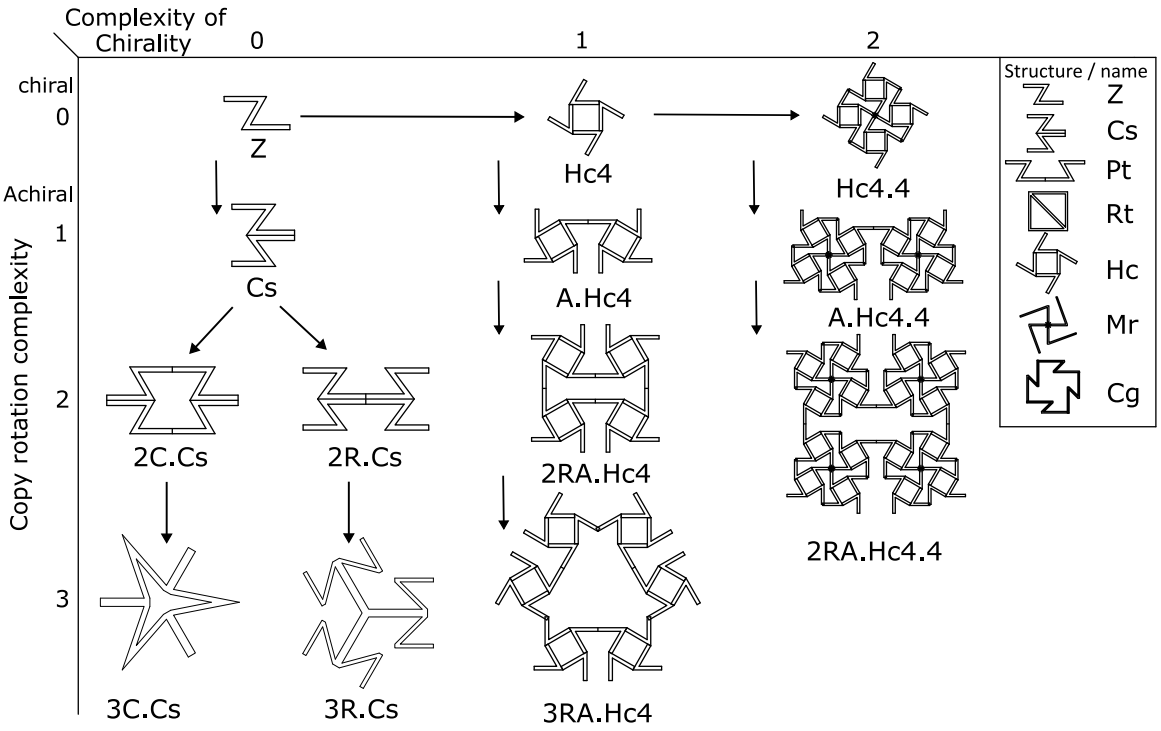

Fig. F.21. Representation of the naming process for the achiral connected stars (Cs) design with the branching of the classical and reciprocal copy-rotation, with two level of copy-rotation complexity. The naming process also shows the chiral Honeycomb (Hc) design with two level of complexity of chirality with two level of copy-rotation complexity.

References

Alderson, A., Alderson, K.L., 2007. Auxetic materials. Proc. Inst. Mech. Eng. G 221 (4), 565–575. http://dx.doi.org/10.1243/09544100JAERO185.

Alderson, A., Alderson, K.L., Attard, D., Evans, K.E., Gatt, R., Grima, J.N., Miller, W., Ravirala, N., Smith, C.W., Zied, K., 2010. Elastic constants of 3-, 4- and 6-connected chiral and anti-chiral honeycombs subject to uniaxial in-plane loading. Compos. Sci. Technol. 70 (7), 1042–1048. http://dx.doi.org/10.1016/j.compscitech.2009.07.009, URL: https://www.sciencedirect.com/science/article/pii/S0266353809002814.

Alderson, K.L., Alderson, A., Smart, G., Simkins, V.R., Davies, P.J., 2002. Auxetic polypropylene fibres:Part 1 - Manufacture and characterisation. Plast. Rubber Compos. 31 (8), 344–349. http://dx.doi.org/10.1179/146580102225006495.

Ali, M.N., Busfield, J.J.C., Rehman, I.U., 2014. Auxetic oesophageal stents: structure and mechanical properties. J. Mater. Sci.: Mater. Med. 25 (2), 527–553. http://dx.doi.org/10.1007/s10856-013-5067-2.

Ali, M.N., Rehman, I.U., 2011. An Auxetic structure configured as oesophageal stent with potential to be used for palliative treatment of oesophageal cancer; development and in vitro mechanical analysis. J. Mater. Sci.: Mater. Med. 22 (11), 2573–2581. http://dx.doi.org/10.1007/s10856-011-4436-y.

Almgren, R., 1985. An isotropic three-dimensional structure with Poisson's ratio = −1. J. Elasticity 15 (4), 427–430. http://dx.doi.org/10.1007/BF00042531.

Attard, D., Farrugia, P.S., Gatt, R., Grima, J.N., 2020. Starchirals–a novel class of auxetic hierarchal structures. Int. J. Mech. Sci. 179, 105631. http://dx.doi.org/10.1016/j.ijmecsci.2020.105631, URL: https://www.sciencedirect.com/science/article/pii/S0020740319341682.

Bessa, M.A., Glowacki, P., Houlder, M., 2019. Bayesian machine learning in metamaterial design: Fragile becomes supercompressible. Adv. Mater. 31 (48), 1904845. http://dx.doi.org/10.1002/adma.201904845, URL: https://onlinelibrary.wiley.com/doi/abs/10.1002/adma.201904845.

Boopathi, B., Ponniah, G., Burela, R.G., 2020. Realizing the impact and compressive strengths of an arrowhead auxetic structure inspired by topology optimization. Int. J. Adv. Eng. Sci. Appl. Math. 12 (3), 211–217. http://dx.doi.org/10.1007/s12572-021-00286-w.

Broeren, F.G.J., Herder, J.L., van der Wijk, V., 2019. On the synthesis of periodic linkages with a specific constant Poisson's ratio. In: Uhl, T. (Ed.), Advances in Mechanism and Machine Science. In: Mechanisms and Machine Science, Springer International Publishing, pp. 249–257. http://dx.doi.org/10.1007/978-3-030-20131-9_25.

Broeren, F.G., van der Wijk, V., Herder, J.L., 2020. Spatial pseudo-rigid body model for the analysis of a tubular mechanical metamaterial. Math. Mech. Solids 25 (2), 305–316. http://dx.doi.org/10.1177/1081286519875500.

Clausen, A., Wang, F., Jensen, J.S., Sigmund, O., Lewis, J.A., 2015. Topology optimized architectures with programmable Poisson's ratio over large deformations. Adv. Mater. 27 (37), 5523–5527. http://dx.doi.org/10.1002/adma.201502485, URL: https://onlinelibrary.wiley.com/doi/abs/10.1002/adma.201502485.

Cuthbert, T.J., Hannigan, B.C., Roberjot, P., Shokurov, A.V., Menon, C., 2023. HACS: Helical auxetic yarn capacitive strain sensors with sensitivity beyond the theoretical limit. Adv. Mater. 35 (10), 2209321. http://dx.doi.org/10.1002/adma.202209321, URL: https://onlinelibrary.wiley.com/doi/abs/10.1002/adma.202209321.

Czajkowski, M., Coulais, C., van Hecke, M., Rocklin, D.Z., 2022. Conformal elasticity of mechanism-based metamaterials. Nature Commun. 13 (1), 211. http://dx.doi.org/10.1038/s41467-021-27825-0, URL: https://www.nature.com/articles/s41467-021-27825-0.

Dagdelen, J., Montoya, J., de Jong, M., Persson, K., 2017. Computational prediction of new auxetic materials. Nature Commun. 8 (1), 323. http://dx.doi.org/10.1038/s41467-017-00399-6, URL: https://www.nature.com/articles/s41467-017-00399-6.

Dirrenberger, J., Forest, S., Jeulin, D., Colin, C., 2011. Homogenization of periodic auxetic materials. Procedia Eng. 10, 1847–1852. http://dx.doi.org/10.1016/j.proeng.2011.04.307, URL: https://www.sciencedirect.com/science/article/pii/S1877705811004954.

Domaschke, S., Morel, A., Fortunato, G., Ehret, A.E., 2019. Random auxetics from buckling fibre networks. Nature Commun. 10 (1), 4863. http://dx.doi.org/10.1038/s41467-019-12757-7, URL: https://www.nature.com/articles/s41467-019-12757-7/.

Duncan, O., Shepherd, T., Moroney, C., Foster, L., Venkatraman, P.D., Winwood, K., Allen, T., Alderson, A., 2018. Review of auxetic materials for sports applications: Expanding options in comfort and protection. Appl. Sci. 8 (6), 941. http://dx.doi.org/10.3390/app8060941, URL: https://www.mdpi.com/2076-3417/8/6/941.

Faraci, D., Driemeier, L., Comi, C., 2021. Bending-dominated auxetic materials for wearable protective devices against impact. J. Dyn. Behav. Mater. 7 (3), 425–435. http://dx.doi.org/10.1007/s40870-020-00284-2.

Fernandez-Corbaton, I., Rockstuhl, C., Ziemke, P., Gumbsch, P., Albiez, A., Schwaiger, R., Frenzel, T., Kadic, M., Wegener, M., 2019. New twists of 3D chiral metamaterials. Adv. Mater. 31 (26), 1807742. http://dx.doi.org/10.1002/adma.201807742, URL: https://onlinelibrary.wiley.com/doi/abs/10.1002/adma.201807742.

Flamourakis, G., Spanos, I., Vangelatos, Z., Manganas, P., Papadimitriou, L., Grigoropoulos, C., Ranella, A., Farsari, M., 2020. Laser-made 3D auxetic metamaterial scaffolds for tissue engineering applications. Macromol. Mater. Eng. 305 (7), 2000238. http://dx.doi.org/10.1002/mame.202000238, URL: https://onlinelibrary.wiley.com/doi/abs/10.1002/mame.202000238.

Frenzel, T., Kadic, M., Wegener, M., 2017. Three-dimensional mechanical metamaterials with a twist. Science 358 (6366), 1072–1074. http://dx.doi.org/10.1126/science.aao4640.

Fu, M.H., Xu, O.T., Hu, L.L., Yu, T.X., 2016. Nonlinear shear modulus of re-entrant hexagonal honeycombs under large deformation. Int. J. Solids Struct. 80, 284–296.

http://dx.doi.org/10.1016/j.ijsolstr.2015.11.015, URL: https://www.sciencedirect.com/science/article/pii/S0020768315004771.

Gao, Y., Wu, Q., Wei, X., Zhou, Z., Xiong, J., 2020. Composite tree-like re-entrant structure with high stiffness and controllable elastic anisotropy. Int. J. Solids Struct. 206, 170–182. http://dx.doi.org/10.1016/j.ijsolstr.2020.09.003, URL: https://www.sciencedirect.com/science/article/pii/S0020768320303413.

Gaspar, N., Ren, X.J., Smith, C.W., Grima, J.N., Evans, K.E., 2005. Novel honeycombs with auxetic behaviour. Acta Mater. 53 (8), 2439–2445. http://dx.doi.org/10.1016/j.actamat.2005.02.006, URL: https://www.sciencedirect.com/science/article/pii/S1359645405000820.

Gatt, R., Mizzi, L., Azzopardi, J.I., Azzopardi, K.M., Attard, D., Casha, A., Briffa, J., Grima, J.N., 2015a. Hierarchical auxetic mechanical metamaterials. Sci. Rep. 5 (1), 8395. http://dx.doi.org/10.1038/srep08395, URL: https://www.nature.com/articles/srep08395.

Gatt, R., Vella Wood, M., Gatt, A., Zarb, F., Formosa, C., Azzopardi, K.M., Casha, A., Agius, T.P., Schembri-Wismayer, P., Attard, L., Chockalingam, N., Grima, J.N., 2015b. Negative Poisson's ratios in tendons: An unexpected mechanical response. Acta Biomater. 24, 201–208. http://dx.doi.org/10.1016/j.actbio.2015.06.018, URL: https://www.sciencedirect.com/science/article/pii/S1742706115002871.

Ge, Z., Hu, H., Liu, S., 2016. A novel plied yarn structure with negative Poisson's ratio. J. Textile Inst. 107 (5), 578–588. http://dx.doi.org/10.1080/00405000.2015.1049069.

Giacomin, J., Scarpa, F., Abderrezak, B., Bullough, W., 2006. Dynamic behavior and damping capacity of auxetic foam pads - art. no. 61690T. Proc. SPIE - Int. Soc. Opt. Eng. 6169, http://dx.doi.org/10.1117/12.658453.

Golomb, S.W., Grunbaum, B., Shephard, G.C., 1988. Tilings and patterns. In: The American Mathematical Monthly, vol. 95, p. 63. http://dx.doi.org/10.2307/2323457, URL: https://www.jstor.org/stable/2323457?origin=crossref.

Gomez-Jauregui, V., Hogg, H., Manchado, C., Otero, C., 2021. GomJau-Hogg's notation for automatic generation of k-uniform tessellations with ANTWERP v3.0. Symmetry 13 (12), 2376. http://dx.doi.org/10.3390/sym13122376, URL: https://www.mdpi.com/2073-8994/13/12/2376.

Grima, J.N., Alderson, A., Evans, K.E., 2005a. Auxetic behaviour from rotating rigid units. Phys. Status Solidi (b) 242 (3), 561–575. http://dx.doi.org/10.1002/pssb.200460376, URL: https://onlinelibrary.wiley.com/doi/abs/10.1002/pssb.200460376.

Grima, J.N., Chetcuti, E., Manicaro, E., Attard, D., Camilleri, M., Gatt, R., Evans, K.E., 2011. On the auxetic properties of generic rotating rigid triangles. Proc. R. Soc. Lond. Ser. A Math. Phys. Eng. Sci. 468 (2139), 810–830. http://dx.doi.org/10.1098/rspa.2011.0273, URL: https://royalsocietypublishing-org.tudelft.idm.oclc.org/doi/10.1098/rspa.2011.0273.

Grima, J.N., Gatt, R., Alderson, A., Evans, K.E., 2005b. On the potential of connected stars as auxetic systems. Mol. Simul. 31 (13), 925–935. http://dx.doi.org/10.1080/08927020500401139.

Hamzehei, R., Kadkhodapour, J., Anaraki, A.P., Rezaei, S., Dariushi, S., Rezadoust, A.M., 2018. Octagonal auxetic metamaterials with hyperelastic properties for large compressive deformation. Int. J. Mech. Sci. 145, 96–105. http://dx.doi.org/10.1016/j.ijmecsci.2018.06.040, URL: https://www.sciencedirect.com/science/article/pii/S0020740318310452.

Houlder, M., Bessa, M., 2019. Design of a super-compressible metamaterial: An experimental investigation guided by machine learning. URL: http://resolver.tudelft.nl/uuid:3716e88c-ea9a-413d-a310-af6cad5009c3.

Hu, H., Zulifqar, A., 2017. Auxetic textile materials - A review. J. Textile Eng. Fashion Technol. Volume 1 (Issue 1), http://dx.doi.org/10.15406/jteft.2017.01.00002, URL: https://medcraveonline.com/JTEFT/JTEFT-01-00002.pdf.

Jang, B., Won, S., Kim, J., Kim, J., Oh, M., Lee, H.-J., Kim, J.-H., 2022. Auxetic metadisplay: Stretchable display without image distortion. Adv. Funct. Mater. 32 (22), 2113299. http://dx.doi.org/10.1002/adfm.202113299, URL: https://onlinelibrary.wiley.com/doi/abs/10.1002/adfm.202113299.

Ji, J.C., Luo, Q., Ye, K., 2021. Vibration control based metamaterials and origami structures: A state-of-the-art review. Mech. Syst. Signal Process. 161, 107945. http://dx.doi.org/10.1016/j.ymssp.2021.107945, URL: https://www.sciencedirect.com/science/article/pii/S088832702100340X.

Jiang, Y., Li, Y., 2017. 3D printed chiral cellular solids with amplified auxetic effects due to elevated internal rotation. Adv. Eng. Mater. 19 (2), 1600609. http://dx.doi.org/10.1002/adem.201600609, URL: https://onlinelibrary.wiley.com/doi/abs/10.1002/adem.201600609.

Jiang, Y., Li, Y., 2018. 3D printed auxetic mechanical metamaterial with chiral cells and re-entrant cores. Sci. Rep. 8 (1), 2397. http://dx.doi.org/10.1038/s41598-018-20795-2, URL: https://www.nature.com/articles/s41598-018-20795-2.

Jiang, Y., Liu, Z., Matsuhisa, N., Qi, D., Leow, W.R., Yang, H., Yu, J., Chen, G., Liu, Y., Wan, C., Liu, Z., Chen, X., 2018. Auxetic mechanical metamaterials to enhance sensitivity of stretchable strain sensors. Adv. Mater. 30 (12), 1706589. http://dx.doi.org/10.1002/adma.201706589, URL: https://onlinelibrary.wiley.com/doi/abs/10.1002/adma.201706589.

Jiang, Y., Rudra, B., Shim, J., Li, Y., 2019. Limiting strain for auxeticity under large compressive Deformation: Chiral vs. re-entrant cellular solids. Int. J. Solids Struct. 162, 87–95. http://dx.doi.org/10.1016/j.ijsolstr.2018.11.035, URL: https://www.sciencedirect.com/science/article/pii/S002076831830489X.

Kadic, M., Milton, G.W., van Hecke, M., Wegener, M., 2019. 3D metamaterials. Nat. Rev. Phys. 1 (3), 198–210. http://dx.doi.org/10.1038/s42254-018-0018-y, URL: https://www.nature.com/articles/s42254-018-0018-y.

Khoshgoftar, M.J., Barkhordari, A., Limuti, M., Buccino, F., Vergani, L., Mirzaali, M.J., 2022. Bending analysis of sandwich panel composite with a re-entrant lattice core using zig-zag theory. Sci. Rep. 12 (1), 15796. http://dx.doi.org/10.1038/s41598-022-19930-x, URL: https://www.nature.com/articles/s41598-022-19930-x.

Kolken, H.M.A., Zadpoor, A.A., 2017. Auxetic mechanical metamaterials. RSC Adv. 7 (9), 5111–5129. http://dx.doi.org/10.1039/C6RA27333E, URL: https://pubs.rsc.org/en/content/articlelanding/2017/ra/c6ra27333e.

Kolpakov, A.G., 1985. Determination of the average characteristics of elastic frameworks. J. Appl. Math. Mech. 49 (6), 739–745. http://dx.doi.org/10.1016/0021-8928(85)90011-5, URL: https://www.sciencedirect.com/science/article/pii/0021892885900115.

Lakes, R., 1987. Foam structures with a negative Poisson's ratio. Science 235 (4792), 1038–1040. http://dx.doi.org/10.1126/science.235.4792.1038.

Lakes, R., 1991. Deformation mechanisms in negative Poisson's ratio materials: structural aspects. J. Mater. Sci. 26 (9), 2287–2292. http://dx.doi.org/10.1007/BF01130170.

Larsen, U., Signund, O., Bouwsta, S., 1997. Design and fabrication of compliant micromechanisms and structures with negative Poisson's ratio. J. Microelectromech. Syst. 6 (2), 99–106. http://dx.doi.org/10.1109/84.585787.

Lee, W., Lee, S., Koh, C., Heo, J., 2010. Moisture sensitive auxetic material. URL: https://patents.google.com/patent/US7858055B2/en.

Lee, J.W., Soman, P., Park, J.H., Chen, S., Cho, D.-W., 2016. A tubular biomaterial construct exhibiting a negative Poisson's ratio. PLoS One 11 (5), e0155681. http://dx.doi.org/10.1371/journal.pone.0155681, URL: https://journals.plos.org/plosone/article?id=10.1371/journal.pone.0155681.

Li, X., Fan, R., Fan, Z., Lu, Y., 2021. Programmable mechanical metamaterials based on hierarchical rotating structures. Int. J. Solids Struct. 216, 145–155. http://dx.doi.org/10.1016/j.ijsolstr.2021.01.028, URL: https://www.sciencedirect.com/science/article/pii/S0020768321000421.

Li, X., Wang, Q., Yang, Z., Lu, Z., 2019. Novel auxetic structures with enhanced mechanical properties. Extreme Mech. Lett. 27, 59–65. http://dx.doi.org/10.1016/j.eml.2019.01.002, URL: https://www.sciencedirect.com/science/article/pii/S2352431618302128.

Li, D., Yin, J., Dong, L., Lakes, R.S., 2018. Strong re-entrant cellular structures with negative Poisson's ratio. J. Mater. Sci. 53 (5), 3493–3499. http://dx.doi.org/10.1007/s10853-017-1809-8.

Lim, T.-C., 2019. Metamaterials with Poisson's ratio sign toggling by means of microstructural duality. SN Appl. Sci. 1 (2), 176. http://dx.doi.org/10.1007/s42452-019-0185-1.

Lim, T.-C., 2020. Auxetic microstructures. In: Lim, T.-C. (Ed.), Mechanics of Metamaterials with Negative Parameters. In: Engineering Materials, Springer, Singapore, pp. 9–51.

Lipton, J.I., MacCurdy, R., Manchester, Z., Chin, L., Cellucci, D., Rus, D., 2018. Handedness in shearing auxetics creates rigid and compliant structures. Science 360 (6389), 632–635. http://dx.doi.org/10.1126/science.aar4586, URL: https://www-science-org.tudelft.idm.oclc.org/doi/10.1126/science.aar4586.

Liu, B., Feng, J., Yu, K., Li, J., Hu, Q., Lin, Z., Fu, J., 2022. Three-dimensional auxetic structure design methods based on bulking-induced deformation and the application in soft crawling robot. Composites B 244, 110146. http://dx.doi.org/10.1016/j.compositesb.2022.110146, URL: https://www.sciencedirect.com/science/article/pii/S1359836822005212.

Liu, Y., Hu, H., 2010. A review on auxetic structures and polymeric materials. Sci. Res. Essays 12.

Liu, S., Yang, Q.-S., Tao, R., Liu, X., 2020. A highly-compressible, torsion-contraction coupling and self-transforming cylindrical bi-material metastructure. Smart Mater. Struct. 29 (2), 025016. http://dx.doi.org/10.1088/1361-665X/ab6078.

Lurie, S.A., Kalamkarov, A.L., Solyaev, Y.O., Ustenko, A.D., Volkov, A.V., 2018. Continuum micro-dilatation modeling of auxetic metamaterials. Int. J. Solids Struct. 132–133, 188–200. http://dx.doi.org/10.1016/j.ijsolstr.2017.09.022, URL: https://www.sciencedirect.com/science/article/pii/S0020768317304328.

Mandelbrot, B.B., 1983. The Fractal Geometry of Nature. Henry Holt and Company.

Mizzi, L., Spaggiari, A., 2022. Novel chiral honeycombs based on octahedral and dodecahedral Euclidean polygonal tessellations. Int. J. Solids Struct. 238, 111428. http://dx.doi.org/10.1016/j.ijsolstr.2022.111428, URL: https://www.sciencedirect.com/science/article/pii/S0020768322000063.

Namvar, N., Moloukzadeh, I., Zolfagharian, A., Demoly, F., Bodaghi, M., 2023. Bio-inspired design, modeling, and 3D printing of lattice-based scale model scooter decks. Int. J. Adv. Manuf. Technol. http://dx.doi.org/10.1007/s00170-023-11185-8.

Ng, W.S., Hu, H., 2017. Tensile and deformation behavior of auxetic plied yarns. Phys. Status Solidi (b) 254 (12), 1600790. http://dx.doi.org/10.1002/pssb.201600790, URL: https://onlinelibrary.wiley.com/doi/abs/10.1002/pssb.201600790.

Olvera, D., Sohrabi Molina, M., Hendy, G., Monaghan, M.G., 2020. Electroconductive melt electrowritten patches matching the mechanical anisotropy of human myocardium. Adv. Funct. Mater. 30 (44), 1909880. http://dx.doi.org/10.1002/adfm.201909880, URL: https://onlinelibrary.wiley.com/doi/abs/10.1002/adfm.201909880.

Papadopoulou, A., Laucks, J., Tibbits, S., 2017. Auxetic materials in design and architecture. Nat. Rev. Mater. 2 (12), 1–3. http://dx.doi.org/10.1038/natrevmats.2017.78, URL: https://www.nature.com/articles/natrevmats201778.

Pasini, D., Rafsanjani Abbasi, A., 2017. Bistable auxetics. URL: https://www.freepatentsonline.com/20170362414.html.

Rafsanjani, A., Pasini, D., 2016. Bistable auxetic mechanical metamaterials inspired by ancient geometric motifs. Extreme Mech. Lett. 9, 291–296. http://dx.doi.org/10.1016/j.eml.2016.09.001, URL: https://www.sciencedirect.com/science/article/pii/S2352431616301298.

Rant, D., Rijavec, T., Pavko-Čuden, A., 2013. Auxetic textiles. J. Acta Chim. Slov. 60 (4), 715–723.

Ren, X., Han, D., Sun, L., Zhang, X.G., Jiang, W., Tao, Z., Xie, Y.M., Yang, F., Lu, G.X., 2023. Experimental and numerical investigations of aluminum foam-filled auxetic circular tubular metamaterials with elliptical cells. Constr. Build. Mater. 374, 130900. http://dx.doi.org/10.1016/j.conbuildmat.2023.130900, URL: https://www.sciencedirect.com/science/article/pii/S0950061823006128.

Shaat, M., Wagih, A., 2020. Hinged-3D metamaterials with giant and strain-independent Poisson's ratios. Sci. Rep. 10 (1), 2228. http://dx.doi.org/10.1038/s41598-020-59205-x, URL: https://www.nature.com/articles/s41598-020-59205-x.

Shen, L., Wang, Z., Wang, X., Wei, K., 2021. Negative Poisson's ratio and effective Young's modulus of a vertex-based hierarchical re-entrant honeycomb structure. Int. J. Mech. Sci. 206, 106611. http://dx.doi.org/10.1016/j.ijmecsci.2021.106611, URL: https://www.sciencedirect.com/science/article/pii/S0020740321003453.

Sloan, M.R., Wright, J.R., Evans, K.E., 2011. The helical auxetic yarn – A novel structure for composites and textiles; geometry, manufacture and mechanical properties. Mech. Mater. 43 (9), 476–486. http://dx.doi.org/10.1016/j.mechmat.2011.05.003, URL: https://www.sciencedirect.com/science/article/pii/S0167663611000913.

Smith, C.W., Grima, J.N., Evans, K.E., 2000. A novel mechanism for generating auxetic behaviour in reticulated foams: missing rib foam model. Acta Mater. 48 (17), 4349–4356. http://dx.doi.org/10.1016/S1359-6454(00)00269-X, URL: https://www.sciencedirect.com/science/article/pii/S135964540000269X.

Stavric, M., Wiltsche, A., 2019. Geometrical elaboration of auxetic structures. Nexus Netw. J. 21 (1), 79–90. http://dx.doi.org/10.1007/s00004-019-00428-5.

Taherkhani, B., Bodaghi, M., Rahmani, S., Mesgari, F., 2023. Novel linear, piezo-resistive, auxetic sensors coated by AAA battery active carbons with supreme sensitivity for human body movement detection. Adv. Eng. Mater. http://dx.doi.org/10.1002/adem.202300524, URL: https://onlinelibrary.wiley.com/doi/abs/10.1002/adem.202300524.

Wang, D., Dong, L., Gu, G., 2022. 3D printed fractal metamaterials with tunable mechanical properties and shape reconfiguration. Adv. Funct. Mater. 33, http://dx.doi.org/10.1002/adfm.202208849.

Wang, X.-T., Wang, B., Li, X.-W., Ma, L., 2017. Mechanical properties of 3D re-entrant auxetic cellular structures. Int. J. Mech. Sci. 131–132, 396–407. http://dx.doi.org/10.1016/j.ijmecsci.2017.05.048, URL: https://www.sciencedirect.com/science/article/pii/S0020740317306239.

Wang, Z., Zulifqar, A., Hu, H., 2016. 7 - Auxetic composites in aerospace engineering. In: Rana, S., Fangueiro, R. (Eds.), Advanced Composite Materials for Aerospace Engineering. Woodhead Publishing, pp. 213–240, URL: https://www.sciencedirect.com/science/article/pii/B9780081000373000079.

Williams, J.L., Lewis, J.L., 1982. Properties and an anisotropic model of cancellous bone from the proximal tibial epiphysis. J. Biomech. Eng. 104 (1), 50–56. http://dx.doi.org/10.1115/1.3138303.

Wu, W., Liu, P., Kang, Z., 2021. A novel mechanical metamaterial with simultaneous stretching- and compression-expanding property. Mater. Des. 208, 109930. http://dx.doi.org/10.1016/j.matdes.2021.109930, URL: https://www.sciencedirect.com/science/article/pii/S0264127521004834.

Wu, W., Song, X., Liang, J., Xia, R., Qian, G., Fang, D., 2018. Mechanical properties of anti-tetrachiral auxetic stents. Compos. Struct. 185, 381–392. http://dx.doi.org/10.1016/j.compstruct.2017.11.048, URL: https://www.sciencedirect.com/science/article/pii/S0263822317324078.

Yao, Y., Ni, Y., He, L., 2023. Unexpected bending behavior of architected 2D lattice materials. Sci. Adv. 9 (25), eadg3499. http://dx.doi.org/10.1126/sciadv.adg3499, URL: https://www.ncbi.nlm.nih.gov/pmc/articles/PMC10284540/.

Yarali, E., Zadpoor, A.A., Staufer, U., Accardo, A., Mirzaali, M.J., 2023. Auxeticity as a mechanobiological tool to create meta-biomaterials. ACS Appl. Bio Mater. http://dx.doi.org/10.1021/acsabm.3c00145.

Ye, X., He, Y., Li, S., Hu, H., Gan, L., Huang, J., 2022. Auxetic wearable sensors based on flexible triboelectric polymers for movement monitoring. ACS Appl. Polym. Mater. 4 (6), 4339–4346. http://dx.doi.org/10.1021/acsapm.2c00309.

Yousefi, A., Jolaiy, S., Lalegani Dezaki, M., Zolfagharian, A., Serjouei, A., Bodaghi, M., 2022. 3D-printed soft and hard meta-structures with supreme energy absorption and dissipation capacities in cyclic loading conditions. Adv. Eng. Mater. 2201189. http://dx.doi.org/10.1002/adem.202201189, URL: https://onlinelibrary.wiley.com/doi/abs/10.1002/adem.202201189.

Zhang, J., Lu, G., You, Z., 2020. Large deformation and energy absorption of additively manufactured auxetic materials and structures: A review. Composites B 201, 108340. http://dx.doi.org/10.1016/j.compositesb.2020.108340, URL: https://www.sciencedirect.com/science/article/pii/S1359836820333898.

Zhang, Y., Ren, X., Jiang, W., Han, D., Yu Zhang, X., Pan, Y., Min Xie, Y., 2022b. In-plane compressive properties of assembled auxetic chiral honeycomb composed of slotted wave plate. Mater. Des. 221, 110956. http://dx.doi.org/10.1016/j.matdes.2022.110956, URL: https://www.sciencedirect.com/science/article/pii/S0264127522005780.

Zhang, X.G., Ren, X., Jiang, W., Zhang, X.Y., Luo, C., Zhang, Y., Xie, Y.M., 2022a. A novel auxetic chiral lattice composite: Experimental and numerical study. Compos. Struct. 282, 115043. http://dx.doi.org/10.1016/j.compstruct.2021.115043, URL: https://www.sciencedirect.com/science/article/pii/S026382232101463X.

Zhang, K., Zhang, X., Gao, Q., Chan, M., Zhang, S., Li, J., Liao, W.-H., 2023. Ultrahigh energy-dissipation and multifunctional auxetic polymeric foam inspired by balloon art. Composites A 167, 107435. http://dx.doi.org/10.1016/j.compositesa.2023.107435, URL: https://www.sciencedirect.com/science/article/pii/S1359835X23000118.

Zhu, Y., Jiang, S., Lu, F., Ren, X., 2022a. A novel enhanced anti-tetra-missing rib auxetic structure with tailorable in-plane mechanical properties. Eng. Struct. 262, 114399. http://dx.doi.org/10.1016/j.engstruct.2022.114399, URL: https://www.sciencedirect.com/science/article/pii/S0141029622005132.

Zhu, Y., Jiang, S., Zhang, Q., Li, J., Yu, C., Zhang, C., 2022b. A novel monoclinic auxetic metamaterial with tunable mechanical properties. Int. J. Mech. Sci. 236, 107750. http://dx.doi.org/10.1016/j.ijmecsci.2022.107750, URL: https://www.sciencedirect.com/science/article/pii/S0020740322006300.